PHYSICAL REVIEW D **95,** 115030 (2017)

Stau coannihilation, compressed spectrum, and SUSY discovery potential at the LHC

Amin Aboubrahim,[*] Pran Nath,[†] and Andrew B. Spisak[‡]

Department of Physics, Northeastern University, Boston, Massachusetts 02115-5000, USA

(Received 17 April 2017; published 26 June 2017)

The lack of observation of supersymmetry thus far implies that the weak supersymmetry scale is larger than what was thought before the LHC era. This observation is strengthened by the Higgs boson mass measurement at ∼125 GeV, which within supersymmetric models implies a large loop correction and a weak supersymmetry scale lying in the several TeV region. In addition if neutralino is the dark matter, its relic density puts further constraints on models often requiring coannihilation to reduce the neutralino relic density to be consistent with experimental observation. The coannihilation in turn implies that the mass gap between the lightest supersymmetric particle and the next to lightest supersymmetric particle will be small, leading to softer final states and making the observation of supersymmetry challenging. In this work we investigate stau coannihilation models within supergravity grand unified models and the potential of discovery of such models at the LHC in the post–Higgs boson discovery era. We utilize a variety of signal regions to optimize the discovery of supersymmetry in the stau coannihilation region. In the analysis presented we impose the relic density constraint as well as the constraint of the Higgs boson mass. The range of sparticle masses discoverable up to the optimal integrated luminosity of the HL-LHC is investigated. It is found that the mass difference between the stau and the neutralino does not exceed ∼20 GeV over the entire mass range of the models explored. Thus the discovery of a supersymmetric signal arising from the stau coannihilation region will also provide a measurement of the neutralino mass. The direct detection of neutralino dark matter is analyzed within the class of stau coannihilation models investigated. The analysis is extended to include multiparticle coannihilation where stau along with chargino and the second neutralino enter into the coannihilation process.

DOI: 10.1103/PhysRevD.95.115030

I. INTRODUCTION

Supersymmetry has not been observed thus far, which implies that its scale is higher than was expected before the LHC era. This observation is strengthened by the discovery that the Higgs boson [1–3] mass is ∼125 GeV [4,5].[1] Analysis within a high-scale supergravity grand unified model [7] (for a review see [8]) shows that the loop correction to the Higgs boson mass in supersymmetry must itself be sizable, which in turn implies a larger value for the weak supersymmetry scale lying in the several TeV region [9–12]. There is another constraint that explains the possible reason for the lack of detection of a supersymmetric signal. In supergravity grand unified models with R parity conservation, neutralino is the lightest supersymmetric particle (LSP) over most of the parameter space of models [13] and thus a candidate for dark matter. The annihilation of the neutralino in sufficient amounts to have its relic density consistent with the WMAP and then Planck experimental results imposes additional constraints. Specifically if the neutralino is binolike, one needs coannihilation (for early work see [14]) to have consistency with experiment. However, coannihilation implies that the next to lightest supersymmetric particle (NLSP) must be close to the LSP with a small mass gap to ensure efficient annihilation of the LSP. The existence of the small mass gap in turn implies that the final states in the decay of the NLSP will be soft, making them difficult to detect. Coannihilation appears in supergravity models with universal as well as with nonuniversal boundary conditions at the grand unification scale which lead to a large sparticle landscape [15]. The large landscape includes nonuniversalities in the gaugino sector [16,17] and in the matter and Higgs sectors [18]. We note in passing that often naturalness criteria are used to argue what the scale of weak scale supersymmetry should be. Previously it has been argued that the weak scale could be large and natural on the hyperbolic branch of radiative breaking of the electroweak symmetry [19–25]. Additionally, analyses of naturalness including proton stability from baryon and lepton number violating dimension 5 operators in grand unified theories (for a review of the status see [26]) along with electroweak symmetry breaking constraints tend to favor the weak scale of supersymmetry (SUSY) in the TeV region [27].

Thus coannihilation necessarily implies that the lightest sparticle spectra which are the prime candidates for

[*]a.abouibrahim@northeastern.edu
[†]p.nath@northeastern.edu
[‡]a.spisak@northeastern.edu

[1]For a review of the status of supersymmetry after the Higgs boson mass measurement at ∼125 GeV see [6].

detection are compressed. Such compressed spectra can appear in stau coannihilation, stop coannihilation, and gluino coannihilation among others (for some recent works on stop coannihilation and gluino coannihilation in the post–Higgs boson discovery era see [28,29]. For recent theoretical papers related to supersymmetry and compressed spectrum see [30–33], and for experimental searches for supersymmetry with a compressed spectrum see [34–36]). In this work we extend that analysis to the stau coannihilation region under the Higgs boson mass constraint and the relic density constraints. Stau-neutralino coannihilation has previously been investigated by a number of works [31,37–40]. Specifically in [31] an analysis has been carried out for the stau-neutralino coannihilation region at LHC Run II. However, the analysis of [31] was limited to neutralino masses below 100 GeV and, further, the Higgs boson mass constraint and the relic density constraints were not imposed. In this work we use nonuniversal supergravity models with nonuniversalities in the gaugino sector to investigate the full range of neutralino and stau masses that are discoverable up to the expected integrated luminosity at the LHC in the future. In our analysis we impose the relic density constraints as well as a constraint of the Higgs boson mass. Specifically we use supergravity model with gluino-dominated radiative breaking ($\tilde{g}$SUGRA) [41], where the mass for the $SU(3)_C$ gaugino is much larger than the masses for the electroweak gauginos. In this case the universal scalar mass can be rather low-lying in the low hundreds of GeV and it is the gluino which drives the radiative breaking, giving much larger masses to the squarks while the slepton masses remain low. In this case the stop masses can be large enough to give the desired loop corrections for the Higgs boson mass. Further, the large splitting between the squark masses and the slepton masses allows for the possibility of a stau-neutralino coannihilation. We will also investigate in the $\tilde{g}$SUGRA framework a multiparticle coannihilation where more than two particles participate in the coannihilation process. This happens, for example, if the neutralino, the stau, and the chargino, and the next to lightest neutralino are clustered together. In this case one finds a more copious set of signatures for discovery. We use signal regions based on those previously published in [40,42] but optimized for the stau-neutralino coannihilation region. An analysis of dark matter is also given. Some of the signatures of the $\tilde{g}$SUGRA model were analyzed in [41] and a more detailed signature analysis and the potential for discovery of this model was given in [43]. Here we analyze the discovery potential of $\tilde{g}$SUGRA for a set of benchmark parameter points with optimization of the signal regions. A comparison of this analysis with some of the previous work is given at the end of Sec. IV C.

The outline of the rest of the paper is as follows: In Sec. II we discuss how a stau-neutralino coannihilation can arise in a high-scale model while generating the desired correction to the Higgs boson mass and also satisfying the relic density constraint. We also discuss here the possibility of a multiparticle coannihilation involving the neutralino, the stau, the chargino, and the second neutralino. In Sec. III, we discuss the production of supersymmetric particles for the stau and the multiparticle coannihilation models. Here we exhibit the cross sections for the production of the final states $\tilde{\chi}_2^0\tilde{\chi}_1^\pm$, $\tilde{\chi}_1^+\tilde{\chi}_1^-$, $\tilde{\tau}^+\tilde{\tau}^-$, and $\tilde{\tau}\tilde{\nu}_\tau$. The sparticles in the final states decay with a neutralino and leptons in the final states. The signature analysis of these requires knowledge of the backgrounds arising from the production and decay of the standard model particles. Here we use the backgrounds published by the Snowmass group. Section IV is devoted to the signature analysis of the high-scale models and an analysis of the minimum integrated luminosity needed with the LHC operating at 13 TeV for the 5σ discovery. Here a comparison of the different signature regions is also made and combined signal region results are exhibited where models are arranged in terms of ascending order in the minimum integrated luminosity needed for a 5σ discovery. At the end of this section we give an analysis of dark matter cross sections for the models discussed in Secs. II–IV. It is shown that the spin-independent neutralino-proton cross sections lie significantly above the neutrino floor and some of the models lie close to the lower bounds that will be reached by the next generation direct detection experiments. Conclusions are given in Sec. V.

II. STAU COANNIHILATION IN SUGRA MODELS

We have earlier noted that the observation of the Higgs boson mass at ∼125 GeV requires a large loop correction to its tree value which is below the Z-boson mass. The largest correction arises from the stop masses in the loop and one needs an average stop mass in the several TeV region. In SUGRA models with universal soft parameters at the grand unification scale, this would indicate a large universal scalar mass m_0 if we wish to have the charginos and the neutralinos at the electroweak scale. A large universal scalar mass would also imply that the sleptons also have few TeV size masses. Thus this setup would not lead to stau coannihilation, which requires that the lightest neutralino, which we assume to be the LSP, and the lighter stau be in proximity to a mass gap so that $(m_{\tilde{\tau}} - m_{\tilde{\chi}^0})/(m_{\tilde{\tau}} + m_{\tilde{\chi}^0}) \leq 1/20$. In high-scale models stau coannihilation can occur with charginos and the neutralinos at the electroweak scale if we lower the universal scalar mass so that the sleptons in general have a mass comparable to the masses of the charginos and the neutralinos. This leads us to nonuniversal SUGRA models of a specific variety, i.e., where we consider nonuniversalities in the gaugino sector—specifically, if we consider the mass of the $SU(3)_C$ gaugino (m_3) at the grand unification scale to be much larger than the masses of the $U(1)_Y$ and $SU(2)_L$ gauginos (m_1, m_2), i.e., $m_3 \gg m_1, m_2$. In this class of models which are labeled $\tilde{g}$SUGRA [41], m_0 is chosen to

TABLE I. Input parameters for representative stau coannihilation benchmark points. All masses are in GeV.

Model	m_0	A_0	$m_1 = m_2$	m_3	$\tan\beta$
(a)	286	−523	314	3015	10
(b)	297	−553	343	3246	10
(c)	267	−378	367	2911	10
(d)	295	−491	381	2821	13
(e)	325	−416	412	3156	14
(f)	317	−497	437	3065	14
(g)	364	−587	445	3728	14
(h)	412	−904	503	4688	13
(j)	337	833	593	3626	15
(k)	295	−551	302	3165	10

be of the relatively low size of a few hundred GeV, while m_3 is taken to be of the relatively large size of several TeV. The large m_3 mass drives the squark masses to acquire TeV size masses through renormalization group evolution (for a review see [44]), while the slepton masses remain largely unaffected [41]. This setup allows one to realize stau coannihilation since both the neutralino and the stau lie in the sub-TeV region and can lie close to each other.

The parameter space of this model is thus given by m_0, A_0, $m_1 = m_2 \ll m_3$, $\tan\beta$, sign(μ), where A_0 is the universal trilinear scalar coupling at the grand unification scale, $\tan\beta = \langle H_2\rangle/\langle H_1\rangle$, where H_2 gives mass to the up quarks and H_1 gives mass to the down quarks and the leptons, and sign(μ) is the sign of the Higgs mixing parameter which enters into the superpotential in the term $\mu H_1 H_2$. For the multiparticle coannihilation parameter space, we relax the requirement that $m_1 = m_2$, allowing m_2 to lie lower than m_1. This brings the mass of the chargino and second neutralino closer to the stau and the LSP so that those particles also contribute to coannihilation. In this case we use the following parameter space for the model: m_0, A_0, $m_2 < m_1 \ll m_3$, $\tan\beta$, sign(μ). Using the above input parameters, the sparticle spectrum is generated using SoftSUSY3.7.3 [45,46] while the analysis of the relic density is done using micrOMEGAs4.3.1 [47]. SUSY Les Houches Accord formatted data files are processed using pySLHA [48].

TABLE III. Input parameters for representative stau-chargino coannihilation benchmark points. All masses are in GeV.

Model	m_0	A_0	m_1	m_2	m_3	$\tan\beta$
(i)	345	68	394	287	3690	10
(ii)	385	152	403	290	3972	12
(iii)	318	248	357	249	2973	12
(iv)	386	−47	401	284	3809	13
(v)	367	78	409	290	3550	13
(vi)	423	−19	431	314	4396	13
(vii)	353	202	427	298	3351	13
(viii)	390	−161	440	308	3864	13
(ix)	321	246	423	296	3328	10
(x)	432	264	494	350	4234	15
(xi)	304	−745	260	221	2793	11

First we consider parameter regions of the $\tilde{g}$SUGRA model with the Higgs boson mass of 125 ± 2 GeV where stau-LSP coannihilation gives rise to a LSP relic density within the known limit $\Omega h^2 < 0.128$. A sample set of such points is given in Tables I and II, where Table I gives the input parameters and Table II gives the sparticle masses for those inputs. As demonstrated in Table II, the parameter points in the stau coannihilation region have a very small stau-neutralino mass gap $\Delta = (m_{\tilde{\tau}_1} - m_{\tilde{\chi}_1^0}) \sim 20\,\text{GeV}$. Such a small gap raises many challenges for discovery. In cases with such little energy available for decay jets, initial (ISR) and final state radiation (FSR) events are often relied upon to produce a more detectible signal at colliders. Next we consider a model of multiparticle coannihilation among the neutralino (LSP), the stau (NLSP), and the chargino and second neutralino, which in this model remain nearly degenerate. The parameter points of Table III are chosen so as to satisfy the constraints on the Higgs boson mass, $m_h = 125 \pm 2$ GeV, and the relic density $\Omega h^2 < 0.128$ and in such a way as to produce the mass hierarchy $m_{\chi_1^0} < m_{\tilde{\tau}} < m_{\chi_1^\pm} \sim m_{\chi_2^0}$. Some of the sparticle masses corresponding to Table III are given in Table IV.

TABLE II. The Higgs boson (h^0) mass, some relevant sparticle masses, and the relic density for the stau coannihilation benchmark points of Table I. All masses are in GeV.

Model	h^0	$\tilde{\tau}$	$\tilde{e}_L$	$\tilde{e}_R$	$\tilde{\mu}_L$	$\tilde{\mu}_R$	$\tilde{\chi}_1^0$	$\tilde{\chi}_1^\pm$	$\tilde{t}$	$\tilde{g}$	Ω
(a)	123.2	134.4	251.5	318.3	251.5	318.3	112.4	208.4	4522	6168	0.125
(b)	123.4	144.3	262.4	333.0	262.4	333.0	123.9	229.7	4842	6608	0.121
(c)	123.1	155.1	269.3	309.0	269.3	309.0	136.5	256.0	4376	5961	0.119
(d)	123.1	163.9	309.9	335.6	309.9	335.6	143.7	270.7	4244	5787	0.115
(e)	123.2	176.7	335.3	367.6	335.3	367.6	155.5	292.2	4720	6428	0.133
(f)	123.3	188.9	346.7	364.7	346.7	364.7	167.3	315.5	4584	6251	0.126
(g)	123.4	190.3	356.4	409.3	356.4	409.3	167.0	312.0	5506	7517	0.125
(h)	123.9	212.0	373.7	464.3	373.7	464.3	187.4	347.6	6775	9287	0.126
(j)	123.7	254.0	423.5	409.2	423.5	409.2	232.9	439.5	5422	7308	0.116
(k)	123.2	121.9	243.7	325.3	243.7	325.3	106.2	195.3	4732	6456	0.072

TABLE IV. The Higgs boson mass, some relevant sparticle masses, and the relic density for the stau-chargino coannihilation benchmark points of Table III. All masses are in GeV.

Model	h^0	$\tilde{\tau}$	$\tilde{e}_L$	$\tilde{e}_R$	$\tilde{\mu}_L$	$\tilde{\mu}_R$	$\tilde{\chi}_1^0$	$\tilde{\chi}_1^\pm$	$\tilde{t}$	$\tilde{g}$	Ω
(i)	123.8	161.4	259.9	382.1	259.9	382.1	142.3	171.7	5511	7468	0.124
(ii)	123.8	166.5	290.6	420.1	290.6	420.1	144.6	169.7	5912	8007	0.127
(iii)	123.2	150.2	265.1	350.3	150.2	265.1	130.4	151.4	4521	6098	0.114
(iv)	123.6	166.9	302.3	420.8	302.3	420.8	145.0	167.9	5677	7698	0.115
(v)	123.6	171.4	300.8	403.7	300.8	403.7	150.2	177.8	5320	7201	0.120
(vi)	123.8	176.5	316.8	459.9	316.8	459.9	154.7	183.9	6488	8808	0.107
(vii)	123.5	179.6	302.2	392.9	302.2	392.9	159.3	188.2	5045	6818	0.117
(viii)	123.8	182.8	314.3	430.1	314.3	430.1	162.2	188.5	5742	7797	0.103
(ix)	123.6	175.1	265.1	363.7	265.1	363.7	157.3	185.9	5011	6773	0.121
(x)	123.5	206.5	358.0	475.6	358.0	475.6	184.0	219.0	6272	8492	0.101
(xi)	123.1	121.6	246.4	327.4	246.4	327.4	89.9	131.5	4212	5756	0.125

In Fig. 1 we exhibit the sparticle mass hierarchies generated by model point (a) of Table I. Here the mass hierarchy of some of the low-lying sparticles is $\tilde{\chi}_1^0 < \tilde{\tau}_1 < \tilde{\chi}_1^0 \simeq \tilde{\chi}_1^\pm < \tilde{\nu}_\tau < \tilde{\nu}_L < \tilde{\ell}_L < \tilde{\tau}_2$. In Fig. 2 we exhibit the sparticle mass hierarchies generated by model point (iii) of Table III. Here the mass hierarchy of some of the low-lying sparticles is similar to that for model point (a) of Table I except that $\tilde{\tau}_1$, $\tilde{\chi}_2^0$, and $\tilde{\chi}_1^\pm$ are very close in mass. As discussed in [15] the sparticle mass hierarchies including the mass gaps contain significant information regarding

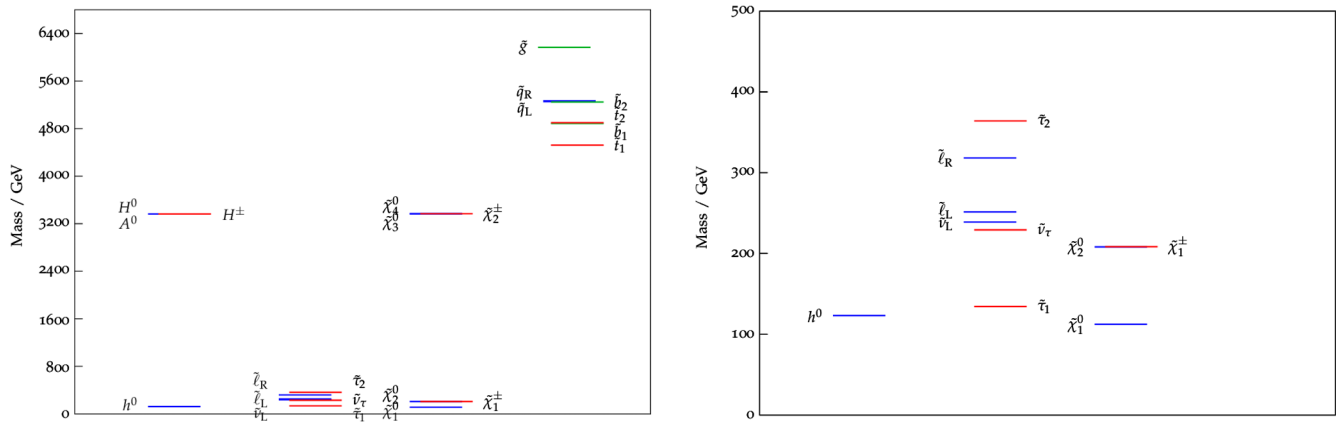

FIG. 1. An exhibition of the sparticle mass hierarchy for stau coannihilation model (a). (Left panel) Full spectrum. (Right panel) Only sparticles with mass < 500 GeV.

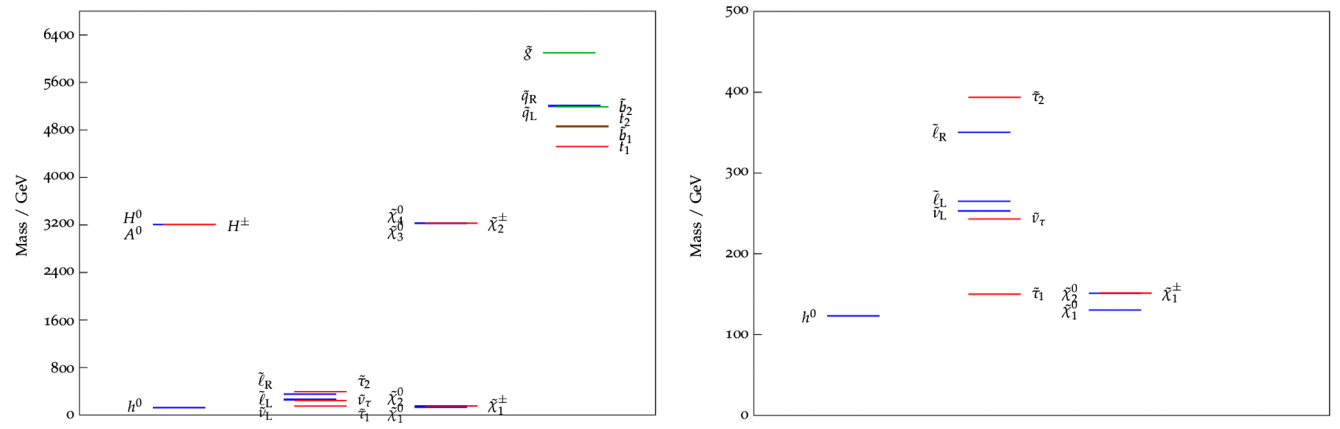

FIG. 2. An exhibition of the sparticle mass hierarchy for multiparticle coannihilation model (iii). (Left panel) Full spectrum. (Right panel) Only sparticles with mass < 500 GeV.

the nature of soft breaking at the grand unification scale, and Figs. 1 and 2 are an illustration of this phenomenon. Thus observation of low-lying sparticles and measurement of their masses will allow us to narrow down in a significant way the nature of the unified model from which the sparticle spectrum originates.

III. ANALYSIS FOR COANNIHILATION MODELS AT LHC AT $\sqrt{s} = 13$ TeV

After a scan of the nonuniversal supergravity parameter space was performed to select benchmark points for each of the two coannihilation models satisfying the Higgs boson mass constraint, the relic density and the desired neutralino, stau, and chargino mass hierarchies discussed in the previous section (Tables I and III), those points are then used for a Monte Carlo analysis of LHC signal regions. This analysis was performed with the MADGRAPH2.4.2 [49] software system. First, the Feynman diagrams were calculated for all possible decays of the form $pp \to$ SUSY SUSY, where "SUSY" can be any minimal supersymmetric standard model (MSSM) particle. The analysis is configured to include both ISR and FSR jets. With the sparticle spectra of the benchmark points calculated by SoftSUSY, as well as the decay widths and branching ratios calculated by SDECAY and HDECAY operating within SUSY-HIT [50], MADEVENT was used to simulate 50,000 MSSM decay events for each benchmark point. Hadronization of the resultant particles is handled by PYTHIA6.4.28 [51], and ATLAS detector simulation and event reconstruction is performed by DELPHES3.3.3 [52]. A large set of search analyses was performed on the generated events for each benchmark point. The analyses used ROOT5.34.21 [53] to implement the constraints of the search region for the signal regions involving hadronic τ final states and other leptonic final states (see Sec. IV).

To allow comparison to the background, all of the signal region analyses were applied to pregenerated backgrounds published by the Snowmass group [54]. For each benchmark point, a calculated implied integrated luminosity allowed direct comparison to the backgrounds. Each individual background process from the Snowmass background set was scaled by its own implied integrated luminosity and combined to determine a total background count for each signal region. The various background samples are grouped according to the generated final state, with a collective notation given by

$$\begin{aligned} J &= \{u, \bar{u}, d, \bar{d}, s, \bar{s}, c, \bar{c}, b, \bar{b}\}, \\ L &= \{e^+, e^-, \mu^+, \mu^-, \tau^+, \tau^-, \nu_e, \nu_\mu, \nu_\tau\}, \\ B &= \{W^+, W^-, Z, \gamma, h^0\}, \\ T &= \{t, \bar{t}\}, \\ H &= \{h^0\}. \end{aligned} \tag{1}$$

In general, events with gauge bosons and the standard model (SM) Higgs boson in the final state are grouped into a single "boson" (B) category. Thus, for example, the data set "Bjj-vbf" represents production via vector boson fusion of a gauge boson or a Higgs boson with at least two additional light-quark jets. The standard model background is displayed for two kinematic variables $M_{\text{eff}}(\text{incl})$ and E_T^{miss} in Fig. 3.

A. LHC production and signal definitions

The signal regions considered here comprise two major categories, based upon the sparticle whose decay signatures they are meant to capture. The first category of signal regions includes signatures based on hadronically decaying taus, which are an expected result of stau decay. The second

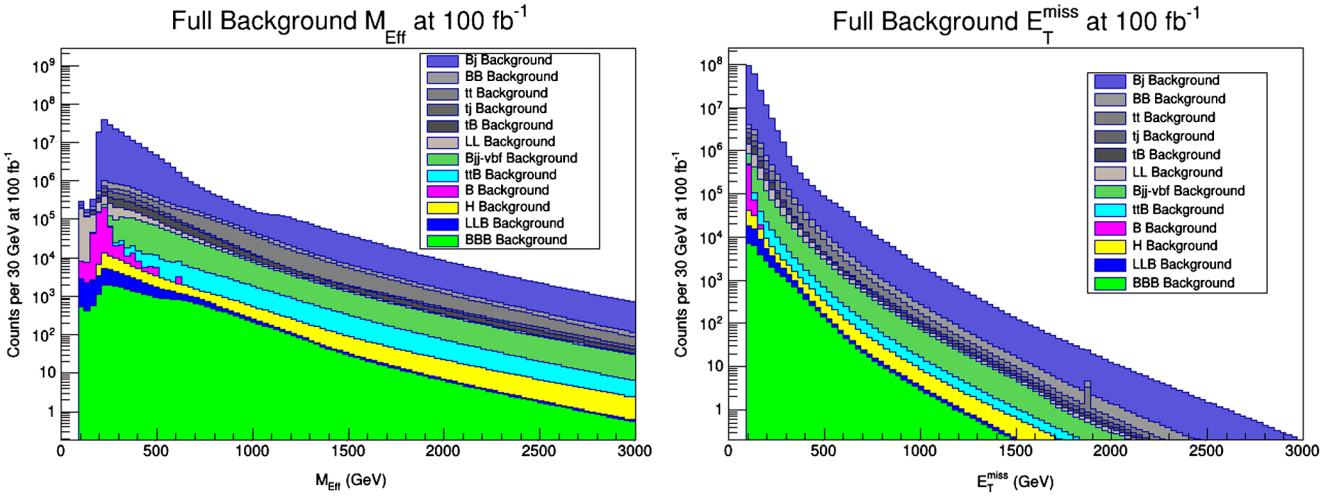

FIG. 3. Full Snowmass standard model background [54] after triggering cuts and a cut of $E_T^{\text{miss}} \geq 100$ GeV, broken into final states and scaled to 100 fb^{-1}. The left panel gives $M_{\text{eff}}(\text{incl})$ and the right panel gives E_T^{miss}. Individual data sets are labeled according to Eq. (1).

category involves signatures of multiple light leptons, which are meant to search for the decays of charginos and heavy neutralinos. Because both of the coannihilation regions under investigation have light staus and electroweak gauginos (i.e., charginos and neutralinos heavier than the lightest neutralino), it is expected that both signal region categories are viable for the stau coannihilation models considered here. The first signal region studied in this work involves at most one hadronically decaying tau in the final state. The selection criteria for one τ_h are based on an optimization of those defined in [40]. The second set of signal regions looks for at most two hadronically decaying taus in the final state. The selection criteria used are a modification of those in [40], where the first (SC1) involves cuts on the transverse momenta of τ_h and the second (SC2) involves cuts on the effective mass, $m_{\rm eff}$, defined as the sum of the missing transverse energy $E_T^{\rm miss}$ and the transverse momenta of the two leading hadronic taus. These signal regions are discussed in greater detail in Sec. IV A. Next we analyze electron and muon signal regions based on the work of [42]. One set of signal regions requires two leptons in the final state, comprising either a same flavor, opposite sign pair or a different flavor, opposite sign pair, with increasing cuts on kinematic variables. The second set requires three leptons in the final state, two of which form a same flavor, opposite sign pair. These are discussed further in Sec. IV B. Using the techniques and signal regions described above, we analyze each of the benchmark points in Tables I and III to identify a signal region with minimum required integrated luminosity for 5σ $S/\sqrt{B}$ discovery of that point at the LHC.

IV. SIGNATURE ANALYSIS AND RESULTS

In Tables V and VI we give an analysis of the sparticle production cross sections for the models under study. The cross section for all models is dominated by the production of the neutralino $\tilde{\chi}_2^0$ and chargino $\tilde{\chi}_1^\pm$. In nearly every model point the only decay mode of $\tilde{\chi}_2^0$ is via the channel $\tilde{\chi}_2^0 \to \tilde{\tau}\tau$, while the primary decay of the chargino is via the channel $\tilde{\chi}_1^\pm \to \tilde{\tau}\nu_\tau$ (see Tables VII and VIII). The stau always decays through one channel, $\tilde{\tau} \to \tilde{\chi}_1^0\tau$ (see Tables IX and X), where the available phase space for the emitted tau is small, resulting in a soft tau production, making it difficult to observe with low integrated luminosity.

TABLE V. SUSY production cross sections in pb for stau coannihilation benchmark points of Table I.

Model	Full SUSY	$\tilde{\chi}_2^0\tilde{\chi}_1^\pm$	$\tilde{\chi}_1^+\tilde{\chi}_1^-$	$\tilde{\tau}^+\tilde{\tau}^-$	$\tilde{\tau}\tilde{\nu}_\tau$
(a)	2.09	2.57	0.62	0.04	0.03
(b)	1.48	0.88	0.43	0.03	0.03
(c)	1.01	0.58	0.29	0.02	0.02
(d)	0.79	0.47	0.23	0.02	0.01
(e)	0.59	0.35	0.17	0.01	0.01
(f)	0.44	0.26	0.13	0.01	0.007
(g)	0.46	0.28	0.13	0.01	0.008
(h)	0.31	0.18	0.09	0.007	0.006
(j)	0.12	0.07	0.03	0.003	0.002
(k)	2.65	1.61	0.79	0.06	0.04

TABLE VI. SUSY production cross sections in pb for multiparticle coannihilation benchmark points of Table III.

Model	Full SUSY	$\tilde{\chi}_2^0\tilde{\chi}_1^\pm$	$\tilde{\chi}_1^+\tilde{\chi}_1^-$	$\tilde{\tau}^+\tilde{\tau}^-$	$\tilde{\tau}\tilde{\nu}_\tau$
(i)	3.99	2.57	1.26	0.02	0.03
(ii)	4.12	2.68	1.32	0.02	0.02
(iii)	6.17	4.02	1.98	0.03	0.03
(iv)	4.25	2.78	1.37	0.02	0.02
(v)	3.48	2.27	1.11	0.02	0.02
(vi)	3.08	2.01	0.98	0.02	0.02
(vii)	2.84	1.84	0.90	0.02	0.01
(viii)	2.81	1.83	0.90	0.01	0.01
(ix)	3.01	1.93	0.94	0.02	0.02
(x)	1.63	1.06	0.52	0.01	0.01
(xi)	10.19	6.65	3.29	0.06	0.04

TABLE VII. Branching ratios for dominant decays of $\tilde{\chi}_1^\pm$ and $\tilde{\chi}_2^0$ for stau coannihilation benchmark points of Table I.

Model	$\tilde{\chi}_2^0 \to \tilde{\tau}\tau$	$\tilde{\chi}_1^\pm \to \tilde{\tau}\nu_\tau$
(a)	1.00	1.00
(b)	1.00	1.00
(c)	0.99	0.99
(d)	1.00	1.00
(e)	1.00	1.00
(f)	1.00	1.00
(g)	1.00	1.00
(h)	0.99	0.99
(j)	0.75	0.75
(k)	1.00	0.99

TABLE VIII. Branching ratios for dominant decays of $\tilde{\chi}_1^\pm$ and $\tilde{\chi}_2^0$ for multiparticle coannihilation benchmark points of Table III.

Model	$\tilde{\chi}_2^0 \to \tilde{\tau}\tau$	$\tilde{\chi}_2^0 \to \tilde{\chi}_1^0\tau^+\tau^-$	$\tilde{\chi}_1^\pm \to \tilde{\tau}\nu_\tau$
(i)	1.00	0.00	1.00
(ii)	1.00	0.00	1.00
(iii)	0.00	0.99	1.00
(iv)	0.00	0.99	1.00
(v)	1.00	0.00	1.00
(vi)	1.00	0.00	1.00
(vii)	1.00	0.00	1.00
(viii)	1.00	0.00	1.00
(ix)	1.00	0.00	1.00
(x)	1.00	0.00	1.00
(xi)	1.00	0.00	1.00

TABLE IX. Branching ratios for dominant decays of $\tilde{\tau}$ and $\tilde{\nu}_\tau$ for stau coannihilation benchmark points of Table I.

Model	$\tilde{\tau} \to \tilde{\chi}_1^0 \tau$	$\tilde{\nu}_\tau \to \tilde{\chi}_1^0 \nu_\tau$	$\tilde{\nu}_\tau \to \tilde{\chi}_2^0 \nu_\tau$	$\tilde{\nu}_\tau \to \tilde{\chi}_1^\pm \tau$	$\tilde{\nu}_\tau \to \tilde{\tau} W^\pm$
(a)	1.00	0.38	0.07	0.13	0.42
(b)	1.00	0.42	0.02	0.03	0.53
(c)	1.00	0.47	0.00	0.00	0.53
(d)	1.00	0.17	0.01	0.03	0.79
(e)	1.00	0.12	0.01	0.02	0.85
(f)	1.00	0.13	0.002	0.004	0.87
(g)	1.00	0.11	0.006	0.13	0.87
(h)	1.00	0.12	0.00	0.00	0.88
(j)	1.00	0.10	0.00	0.00	0.90
(k)	1.00	0.31	0.08	0.15	0.46

TABLE X. Branching ratios for dominant decays of $\tilde{\tau}$ and $\tilde{\nu}_\tau$ for multiparticle coannihilation benchmark points of Table III.

Model	$\tilde{\tau} \to \tilde{\chi}_1^0 \tau$	$\tilde{\nu}_\tau \to \tilde{\chi}_1^0 \nu_\tau$	$\tilde{\nu}_\tau \to \tilde{\chi}_2^0 \nu_\tau$	$\tilde{\nu}_\tau \to \tilde{\chi}_1^\pm \tau$	$\tilde{\nu}_\tau \to \tilde{\tau} W^\pm$
(i)	1.00	0.16	0.27	0.56	0.00
(ii)	1.00	0.11	0.23	0.46	0.20
(iii)	1.00	0.12	0.25	0.51	0.12
(iv)	1.00	0.09	0.20	0.41	0.30
(v)	1.00	0.10	0.21	0.42	0.28
(vi)	1.00	0.09	0.18	0.37	0.36
(vii)	1.00	0.11	0.22	0.44	0.23
(viii)	1.00	0.09	0.20	0.41	0.29
(ix)	1.00	0.18	0.27	0.55	0.00
(x)	1.00	0.07	0.15	0.30	0.48
(xi)	1.00	0.12	0.23	0.47	0.18

A. τ-based signals

We start by discussing the 1τ signature search by applying the selection criteria given in [40]. It turns out that the calculated luminosity necessary for a 5σ discovery lies beyond the maximum integrated luminosity achievable at the LHC. The main problem is the cut on the missing transverse energy. In [40], a cut on $E_T^{\rm miss}$ was made so that $E_T^{\rm miss} > 230$ GeV. However, for the class of models we consider this cut is not optimal as illustrated in the left panel of Fig. 4. Here one finds that we begin to lose the signal for $E_T^{\rm miss} > 200$ GeV leading to a small signal to background ratio in this case. Further, the cut on $p_T(\tau_h)$ of [40], i.e., $15 < p_T(\tau_h) < 35$ GeV, applied on the hadronic tau transverse momentum is not optimal for the models considered here. The right panel of Fig. 4 shows that the signal is above the background in the range 20–90 GeV. Thus increasing the range of the cut on $p_T(\tau_h)$ will produce better results. The optimized cuts for the 1τ signature are displayed in Table XI including three variations: 1τ-A, 1τ-B, and 1τ-C. They correspond to variations of the cut on $p_T(\tau_h)$. Table XII gives the minimum integrated luminosity needed for a 5σ discovery using these cuts on each of the benchmark points of Table III which correspond to the multipartcle coannihilation region. The best results are obtained for the cuts of 1τ-A where the luminosity ranges from 1510 to 2650 fb^{-1}, which is less than the optimal integrated luminosity achievable at the LHC, i.e., ~3000 fb^{-1}. Results obtained from 1τ-C show, for the most part, luminosities greater than 3000 fb^{-1} since the range of the cut on $p_T(\tau_h)$ extends to 150 GeV, which is above the value at which the signal generally begins dropping below background.

Another τ signature of interest is that of two hadronically decaying taus in the final state. Here we adopt the signal regions of Table XI to the 2τ case by considering two selection criteria, SC1 and SC2, as shown in Table XIII. The first selection criterion SC1 is a duplication of the cuts from Table XI, modified to require a second τ, while in the selection criterion SC2 we introduce the variable $m_{\rm eff}$,

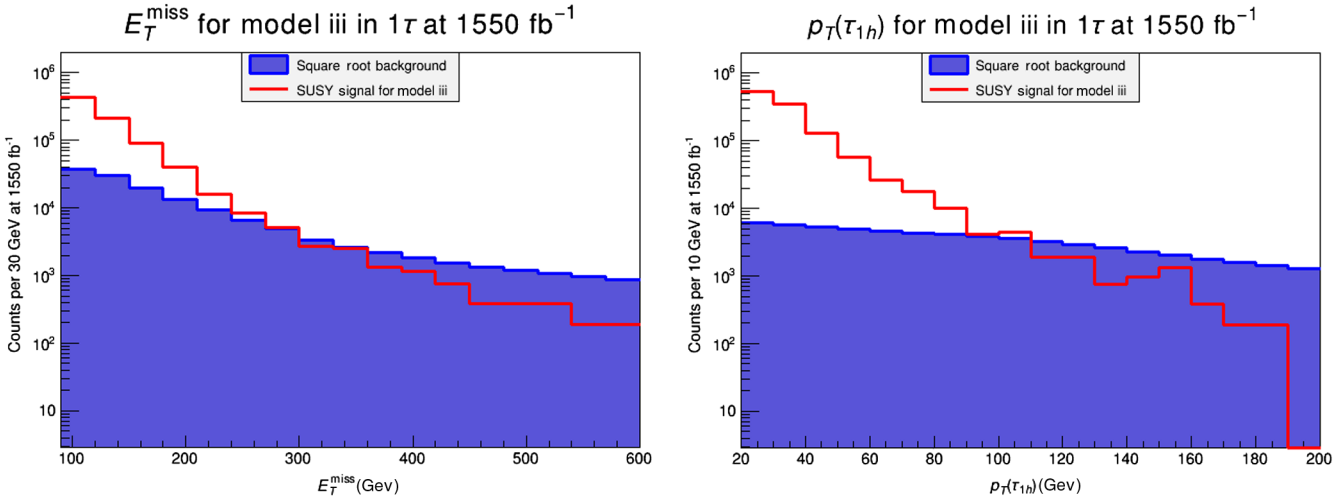

FIG. 4. (Left panel) Distribution in $E_T^{\rm miss}$ for the 1τ signal region for multiparticle coannihilation model (iii) prior to any cuts. Plotted is the number of counts for the SUSY signal per 30 GeV and the square root of the total SM Snowmass background. The analysis is done at 1550 fb^{-1} of integrated luminosity, which gives a 5σ discovery in this signal region. (Right panel) The same analysis as in the left panel but for $p_T(\tau_h)$ with counts per 10 GeV.

TABLE XI. The selection criteria used for the signal regions with one hadronically decaying tau in the final state and a veto on electrons, muons, and b-jets. The angles are in rad.

	Value		
Requirement	1τ-A	1τ-B	1τ-C
$E_T^{\rm miss}$(GeV) >	130	130	130
$p_T(j_1)$(GeV) >	100	100	100
$\lvert\eta(j_1)\rvert$ <	2.5	2.5	2.5
$p_T(\tau_h)$(GeV) >	15	15	20
$p_T(\tau_h)$(GeV) <	50	80	150
$\lvert\eta(\tau_h)\rvert$ <	2.3	2.3	2.3
$\Delta R(\tau_h, j_1)$ >	0.4	0.4	0.4

TABLE XII. Analysis of the discovery potential for supersymmetry for the parameter space of Table III, using the selection criteria of Table XI, where the minimum integrated luminosity needed for 5σ discovery is given in fb^{-1}. Here and in the tables following $\cdots$ indicates that the minimum integrated luminosity needed for 5σ discovery exceeds 3000 fb^{-1}.

Model	$\mathcal{L}$ for 5σ discovery in 1τ-A	$\mathcal{L}$ for 5σ discovery in 1τ-B	$\mathcal{L}$ for 5σ discovery in 1τ-C
(i)	1510	1810	2520
(ii)	1550	1800	2630
(iii)	1550	1910	2730
(iv)	1580	2020	2930
(v)	1800	2260	$\cdots$
(vi)	2010	2290	$\cdots$
(vii)	2010	2330	$\cdots$
(viii)	2090	2340	$\cdots$
(ix)	2400	2880	$\cdots$
(x)	2650	$\cdots$	$\cdots$
(xi)	1610	1420	1720

defined as the scalar sum of the missing transverse energy and the transverse momenta of the two leading hadronic taus, $m_{\rm eff} = E_T^{\rm miss} + p_T^{\tau_{1h}} + p_T^{\tau_{2h}}$. For completeness, we apply those cuts also to the 1τ signal regions and find that this improves our results from Table XII. Thus, the new set of τ-based signal regions after inclusion of additional selection criteria SC1 and SC2 are presented in Table XIII. Here we veto electrons, muons, and b-jets. In this set, we have removed the cut on the pseudorapidity of the leading jet, which was among the cuts for the 1τ signature in Table XI. Also, an upper bound has been placed on the $E_T^{\rm miss}$ cut to suppress values where the signal drops below the background. In Fig. 5 we exhibit the distributions in $p_T(j_1)$, the transverse momentum of the leading jet, and the effective mass $m_{\rm eff}$ for the model point (xi). The signal appears to be above the background for the lower $p_T(j_1)$ and $m_{\rm eff}$ values at which the cuts were applied (Table XIII).

TABLE XIII. The selection criteria (SC) used for the signal regions with the 1τ and 2τ signatures. The SRs SC1 and SC2 have a common cut on the missing transverse energy of 100 GeV < $E_T^{\rm miss}$ < 200 GeV, with a veto on electrons, muons, and b-jets. Empty cells indicate that the kinematical variable is not applicable to the corresponding SR. The angles are in rad.

	SC1					
Requirement	1τ-A	1τ-B	1τ-C	2τ-A	2τ-B	2τ-C
$p_T(j_1)$(GeV) >	20	20	20	20	20	20
$p_T(j_1)$(GeV) <	100	100	100	100	100	100
$p_T(\tau_{1h})$(GeV) >	20	20	20	20	20	20
$p_T(\tau_{1h})$(GeV) <	50	70	90	50	70	90
$p_T(\tau_{2h})$(GeV) >				20	20	20
$p_T(\tau_{2h})$(GeV) <				40	50	60
$\lvert\eta(\tau_{1h})\rvert$ <	1.2	1.2	1.2	1.2	1.2	1.2
$\lvert\eta(\tau_{2h})\rvert$ <				1.0	1.0	1.0
$\Delta R(\tau_{1h}, j_1)$ >	0.6	0.6	0.6	0.6	0.6	0.6
$\Delta R(\tau_{1h}, j_1)$ <	1.8	1.8	1.8	1.8	1.8	1.8
$\Delta R(\tau_{2h}, j_1)$ >				2.3	2.3	2.3
$\Delta R(\tau_{2h}, j_1)$ <				3.3	3.3	3.3
$N(\tau_h)$	1	1	1	2	2	2
	SC2					
Requirement	1τ-A	1τ-B	1τ-C	2τ-A	2τ-B	2τ-C
$p_T(j_1)$(GeV) >	20	20	20			
$p_T(j_1)$(GeV) <	200	200	200	110	110	110
$\lvert\eta(\tau_{1h})\rvert$ <	1.2	1.2	1.2	1.4	1.4	1.4
$\lvert\eta(\tau_{2h})\rvert$ <				1.0	1.0	1.0
$\Delta R(\tau_{1h}, j_1)$ >	0.6	0.6	0.6	0.8	0.8	0.8
$\Delta R(\tau_{1h}, j_1)$ <	1.8	1.8	1.8	1.8	1.8	1.8
$\Delta R(\tau_{2h}, j_1)$ >				2.3	2.3	2.3
$\Delta R(\tau_{2h}, j_1)$ <				3.3	3.3	3.3
$m_{\rm eff}$ >	120	130	140	110	110	110
$m_{\rm eff}$ <	200	250	300	250	350	450
$N(\tau_h)$	1	1	1	2	2	2

In Table XIV we give the required minimum integrated luminosities for discovery for points (a)–(k) corresponding to the stau coannihilation model. The 1τ signature performs better than the 2τ for both SRs, SC1 and SC2, which is the reason this channel was omitted from Table XIV. In 1τSC1 and 1τSC2 all points perform well except (h) and (j). This is because both have the lowest production cross section (see Table V) and thus require higher integrated luminosities for discovery. Point (k) has the lowest integrated luminosity of 220 fb^{-1} in 1τSC1-C and point (d) has the highest at 2960 fb^{-1} in 1τSC1-A. Similarly, we computed the integrated luminosities for benchmark points (i)–(xi) corresponding to the multiparticle coannihilation model. Focusing on the 1τ signature, we notice an improvement compared to what was presented in Table XII. Here all luminosities appear to be well below 3000 fb^{-1} in both SC1 and SC2 and are, thus, within reach of the HL-LHC. Despite having a poorer performance, the 2τ SR and in particular 2τSC2-A gives the lowest luminosity of 73 fb^{-1} for point (xi). It is worth noting that 70% of points (i)–(xi)

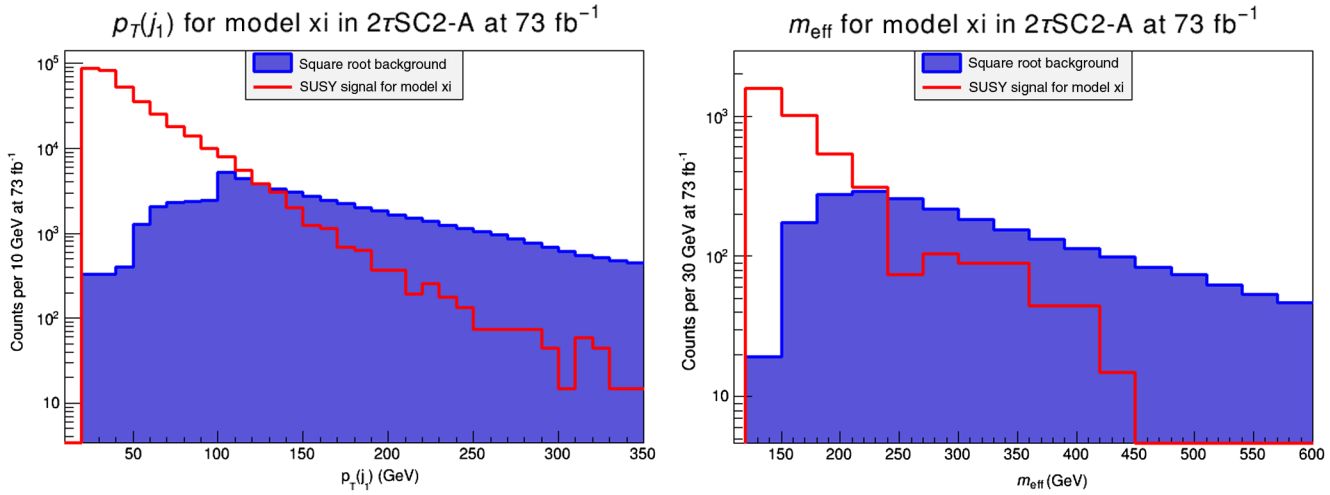

FIG. 5. (Left panel) Distribution in $p_T(j_1)$ for the 2τSC2-A signal region for multiparticle coannihilation model (xi) prior to any cuts. Plotted is the number of counts for the SUSY signal per 10 GeV and the square root of the total SM Snowmass backgrounds. The analysis is done at 73 fb^{-1} of integrated luminosity, which gives a 5σ discovery in this signal region. (Right panel) The same analysis as in the left panel but for m_{eff} with counts for the SUSY signal per 30 GeV.

have 1τSC1-C as the leading SR, while 75% of points (a)–(k) that are listed have 1τSC1-C as the leading SR. It can be seen that introducing the kinematic variable m_{eff} has improved our results for some regions, while it did not have much effect on others. For example, in 2τSC2-A, -B, and -C, where this variable is considered, an integrated luminosity less than 100 fb^{-1} is obtained for point (xi), which can be reached by the end of the current LHC run. In addition, for equivalent kinematic cuts, signal regions demanding a single hadronically decaying tau performed better than those demanding two taus for both the multiparticle coannihilation and stau coannihilation regions. It must be noted that the slight differences between the 1τ and 2τ cuts in SC2 are needed to give plausible results for the 2τ channel. Forcing exactly the same cuts produces overall unsatisfactory results for the 2τ channel. Analysis of the discovery potential for supersymmetry for the parameter space of Table III, using the selection criteria of Table XIII, where the minimum integrated luminosity needed for 5σ discovery is displayed in Table XV.

The last SR we will investigate for the 2τ-based signal is SR-2τSC3, given in Table XVI. The reason for doing so is to try and accommodate most of the variables used by ATLAS in their searches. One of those variables is the quantity $m_{\mathrm{T}\tau 1} + m_{\mathrm{T}\tau 2}$ defined as the sum of the transverse masses of the leading and subleading taus, where $m_{\mathrm{T}\tau}$ is calculated from the transverse momentum of the tau and $\mathbf{p}_{\mathrm{T}}^{\mathrm{miss}}$, so that

$$m_{\mathrm{T}\tau}(\mathbf{p}_{\mathrm{T}\tau}, \mathbf{p}_{\mathrm{T}}^{\mathrm{miss}}) = \sqrt{2(p_{\mathrm{T}\tau} E_{\mathrm{T}}^{\mathrm{miss}} - \mathbf{p}_{\mathrm{T}\tau} \cdot \mathbf{p}_{\mathrm{T}}^{\mathrm{miss}})}, \quad (2)$$

and $\Delta R(\tau_h, \tau_h)$ is the separation between the first two leading taus. Also here we keep our veto on the b-jets, electrons, and muons. Table XVII shows the integrated luminosities obtained for three variations of the transverse mass sum pertaining to the multiparticle coannihilation model points (i)–(xi). Signal region 2τSC3-A gives integrated luminosities as low as 670 fb^{-1} [for point (xi)]. However, more than half of the listed points in Table XVII have 2τSC3-B as their leading SR. It is clear that for the most part, SC1 and SC2 give better results.

In Figs. 5–7 we exhibit the distributions in different kinematical variables for the multiparticle coannihilation model (xi) at 73 fb^{-1} for signal region 2τSC2-A and at 670 fb^{-1} for signal region 2τSC3-A in Fig. 8, where we plot the number of SUSY signal events (red) against the square root of the SM background (blue). The left panel of

TABLE XIV. Analysis of the discovery potential for supersymmetry for the parameter space of Table I, using the selection criteria of Table XIII, where the minimum integrated luminosity needed for 5σ discovery is given in fb^{-1}. Points (h) and (j) are not listed because the integrated luminosity for discovery exceeds 3000 fb^{-1}. Only 1τ signal regions are displayed, as those are the signal regions which give luminosities for discovery in the reasonable range.

	$\mathcal{L}$ for 5σ discovery in SC1			$\mathcal{L}$ for 5σ discovery in SC2		
Model	1τ-A	1τ-B	1τ-C	1τ-A	1τ-B	1τ-C
(a)	786	487	303	745	383	313
(b)	1310	674	416	1120	621	536
(c)	2760	1280	756	2460	1340	1020
(d)	2960	1490	967	2840	1470	1050
(e)	⋯	2860	1700	⋯	2170	1660
(f)	⋯	⋯	2210	⋯	⋯	2340
(g)	⋯	⋯	2460	⋯	⋯	2340
(k)	427	279	220	644	349	299

TABLE XV. Analysis of the discovery potential for supersymmetry for the parameter space of Table III, using the selection criteria of Table XIII, where the minimum integrated luminosity needed for 5σ discovery is given in fb^{-1}. Empty cells indicate that zero events have passed the applied cuts.

	$\mathcal{L}$ for 5σ discovery in SC1						$\mathcal{L}$ for 5σ discovery in SC2					
Model	1τ-A	1τ-B	1τ-C	2τ-A	2τ-B	2τ-C	1τ-A	1τ-B	1τ-C	2τ-A	2τ-B	2τ-C
(i)	1020	704	625	1090	2460	1290	1040	715	694	477	579	582
(ii)	501	380	292				536	370	352			
(iii)	637	512	472	458	1030	542	827	669	648	200	243	244
(iv)	677	575	532				941	695	666	...	...	...
(v)	654	475	411	1440	1440	1710	1070	894	898	631	765	770
(vi)	898	853	650				1170	743	693	1810	2200	2210
(vii)	730	605	508	...	...	...	1190	825	870	...	...	...
(viii)	1040	746	660	2200	...	2060	1250	889	842	2170	1170	1170
(ix)	1190	713	661	...	...	...	1610	1020	1020	842	575	578
(x)	1430	1230	1090	...	...	...	1950	1340	1270	2880	...	...
(xi)	265	169	144	168	378	199	176	143	119	73	89	90

TABLE XVI. The selection criteria used for the signal regions SR-SC3 with two hadronically decaying taus in the final state $[N(\tau_h) = 2]$ and a veto on electrons, muons, and b-jets.

	SR-SC3		
Requirement	2τ-A	2τ-B	2τ-C
$E_T^{\rm miss}$(GeV) >	100	100	100
$E_T^{\rm miss}$(GeV) <	200	200	200
$p_T(j_1)$(GeV) <	180	180	180
$m_{\rm eff}$(GeV) >	130	130	130
$m_{\rm eff}$(GeV) <	200	200	200
$m_{T\tau 1} + m_{T\tau 2}$ >	100	100	50
$m_{T\tau 1} + m_{T\tau 2}$ <	200	300	500
$\Delta R(\tau_h, \tau_h)$ >	2.5	2.5	2.5
$\Delta R(\tau_h, \tau_h)$ <	3.5	3.5	3.5

TABLE XVII. Analysis of the discovery potential for supersymmetry for the parameter space of Table III, using the selection criteria of Table XVI, where the minimum integrated luminosity needed for 5σ discovery is given in fb^{-1}. Models (iv), (vi), and (ix) are not listed because the minimum integrated luminosity needed for 5σ discovery exceeded 3000 fb^{-1}.

Model	$\mathcal{L}$ for 5σ discovery in 2τ-SC3-A	$\mathcal{L}$ for 5σ discovery in 2τ-SC3-B	$\mathcal{L}$ for 5σ discovery in 2τ-SC3-C
(i)	1240	1090	1430
(ii)	1820	1560	1720
(iii)	1170	1180	1730
(v)	1640	1450	2130
(vii)	1710	1540	2270
(viii)	2870	2510	...
(x)	2690	2700	...
(xi)	670	674	991

Fig. 5 shows the distribution in the transverse momentum of the leading jet, $p_T(j_1)$, and the right panel shows the distribution in the effective mass $m_{\rm eff}$. A similar analysis is done in Fig. 6 for the transverse momentum of the leading hadronic tau, $p_T(\tau_{1h})$ (left panel), and subleading $p_T(\tau_{2h})$ (right panel). In Fig. 7 the same analysis is done, but for the spatial separation between the subleading hadronic jet and the leading jet, $\Delta R(\tau_{2h}, j_1)$ in the left panel and the missing transverse energy $E_T^{\rm miss}$ in the right panel. The histogram for the sum of the transverse masses of the first two leading hadronic tau jets is shown in the left panel of Fig. 8 and the histogram for the spatial separation between the two leading hadronic taus $\Delta R(\tau_h, \tau_h)$, which is effective in discriminating against back-to-back events such as multijet production or Z decays, is exhibited in the left panel. The distributions for two kinematical variables are also plotted for point (iii) in the 2τ channel exhibited in Fig. 9 and showing an excess of the signal over background events.

B. e- and μ-based signals

In addition to the direct production of τ leptons due to the decay of stau particles, it is expected that decays of charginos and heavy neutralinos will result in detectible light leptons (electrons and muons) upon which further signal regions can be based. To evaluate the effectiveness of these types of searches in regions of stau coannihilation and multiparticle coannihilation, benchmark models of Tables I and III are evaluated against electroweak gaugino signals designed to search for decays of $\tilde{\chi}_1^+\tilde{\chi}_1^-$ and $\tilde{\chi}_1^\pm\tilde{\chi}_2^0$ [42]. These signal regions are classified according to the number of signal leptons. In the two lepton case, six signal regions are defined in two broad categories (see Table XVIII): signal regions labeled as 2l-SF require that the signal leptons form a same flavor, opposite sign (SFOS) pair, while signal regions labeled as 2l-DF require a different flavor, opposite sign (DFOS) pair. The subcategories A, B, and C in

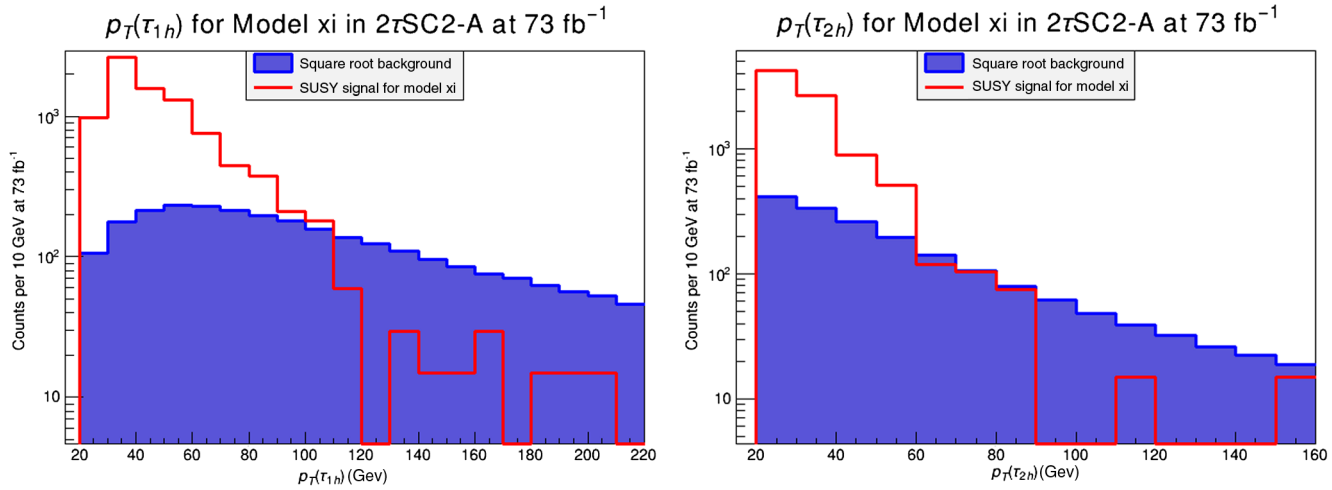

FIG. 6. (Left panel) Distribution in $p_T(\tau_{1h})$ for the 2τSC2-A signal region for the multiparticle coannihilation model (xi) prior to any cuts. Plotted is the number of counts for the SUSY signal per 10 GeV and the square root of the total SM Snowmass backgrounds. The analysis is done at 73 fb^{-1} of integrated luminosity, which gives a 5σ discovery in this signal region. (Right panel) The same analysis as in the left panel but for $p_T(\tau_{2h})$.

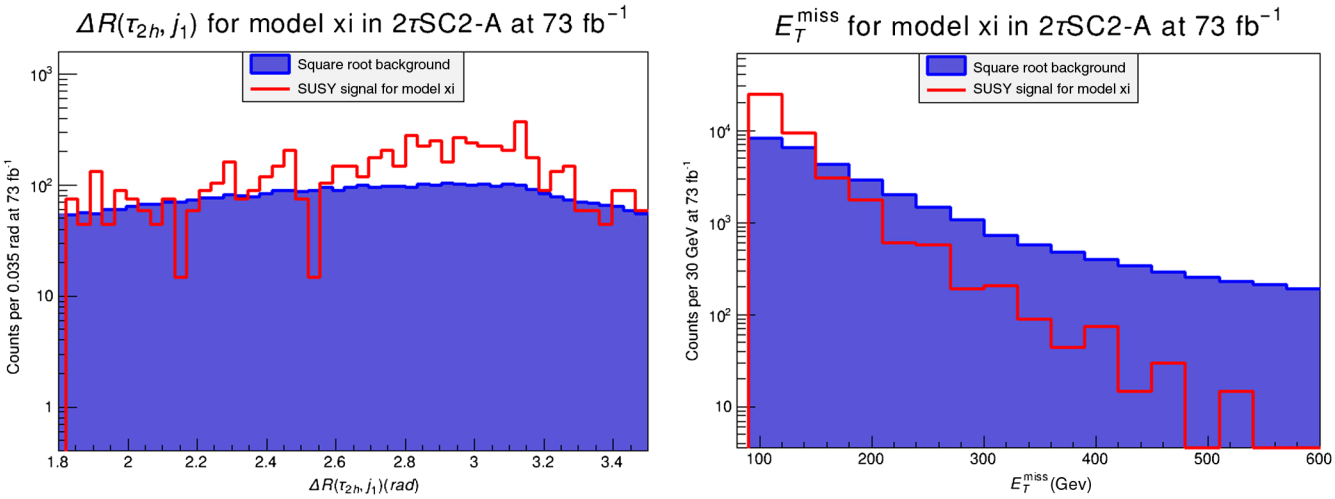

FIG. 7. (Left panel) Distribution in $\Delta R(\tau_{2h}, j_1)$ for the 2τSC2-A signal region for the multiparticle coannihilation model (xi) prior to any cuts. Plotted is the number of counts for the SUSY signal per 0.035 rad and the square root of the total SM Snowmass backgrounds. The analysis is done at 73 fb^{-1} of integrated luminosity, which gives a 5σ discovery in this signal region. (Right panel) The same analysis as in the left panel but for $E_T^{\rm miss}$ with counts for the SUSY signal per 30 GeV.

Table XVIII indicate different cuts on the kinematic variable $m_{\rm T2}$ [55–57], which is defined as

$$m_{\rm T2} = \min\left[\max\left(m_{\rm T}(\mathbf{p}_{\rm T}(\ell_1), \mathbf{q}_{\rm T}), m_{\rm T}(\mathbf{p}_{\rm T}(\ell_2), \mathbf{p}_{\rm T}^{\rm miss} - \mathbf{q}_{\rm T})\right)\right], \tag{3}$$

where $\mathbf{q}_{\rm T}$ is an arbitrary vector chosen to find the appropriate minimum and $m_{\rm T}$ is the transverse mass given by

$$m_{\rm T}(\mathbf{p}_{\rm T1}, \mathbf{p}_{\rm T2}) = \sqrt{2(p_{\rm T1}p_{\rm T2} - \mathbf{p}_{\rm T1}\cdot\mathbf{p}_{\rm T2})}. \tag{4}$$

In addition to cutting on $m_{\rm T2}$ and the missing transverse energy $E_T^{\rm miss}$, the three lepton signal regions contain three jet vetoes, requiring that events contain no jets other than very soft jets in three jet categories: b-tagged jets (b-jet veto), jets which are not b-tagged and which have $|\eta| \leq 2.4$ (light jet veto), and jets which are not b-tagged and which have $2.4 \leq |\eta| \leq 4.5$ (forward jet veto). Finally, for the 2l-SF signal regions, there is a Z veto which requires that the invariant mass of the SFOS lepton pair not lie within 10 GeV of the Z mass. The p_T's of the leading and subleading leptons are required to exceed 25 and 20 GeV, respectively. For the three lepton case, two of the leptons

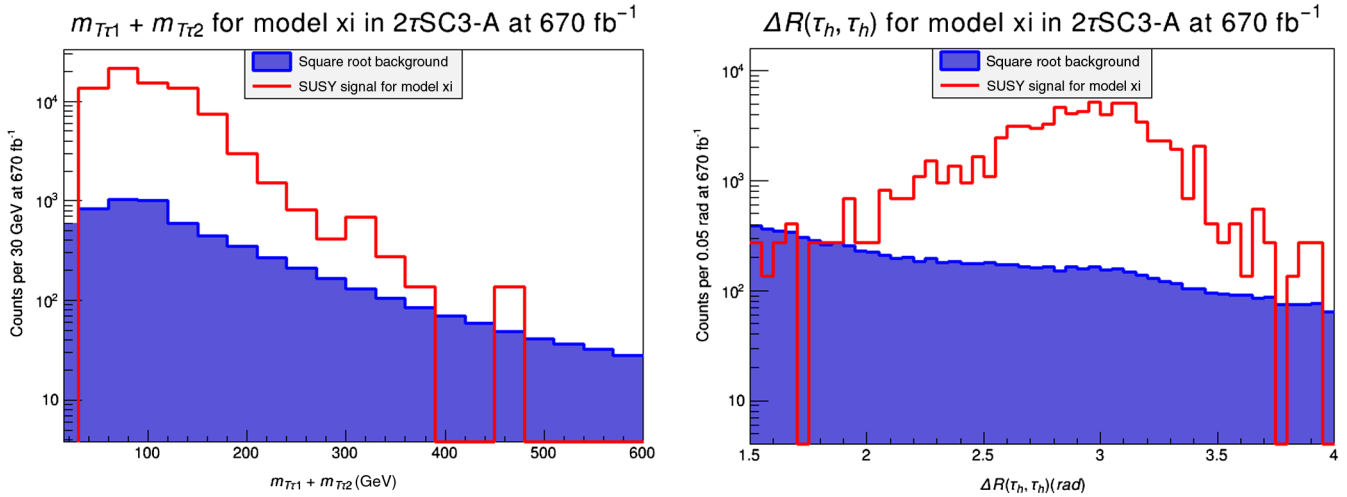

FIG. 8. (Left panel) Distribution in $m_{T\tau 1} + m_{T\tau 2}$ for the 2τSC3-A signal region for the multiparticle coannihilation model (xi) prior to any cuts. Plotted is the number of counts for the SUSY signal per 30 GeV and the square root of the total SM Snowmass backgrounds. The analysis is done at 670 fb^{-1} of integrated luminosity, which gives a 5σ discovery in this signal region. (Right panel) The same analysis as in the left panel but for $\Delta R(\tau_h, \tau_h)$ with counts for the SUSY signal per 0.05 rad.

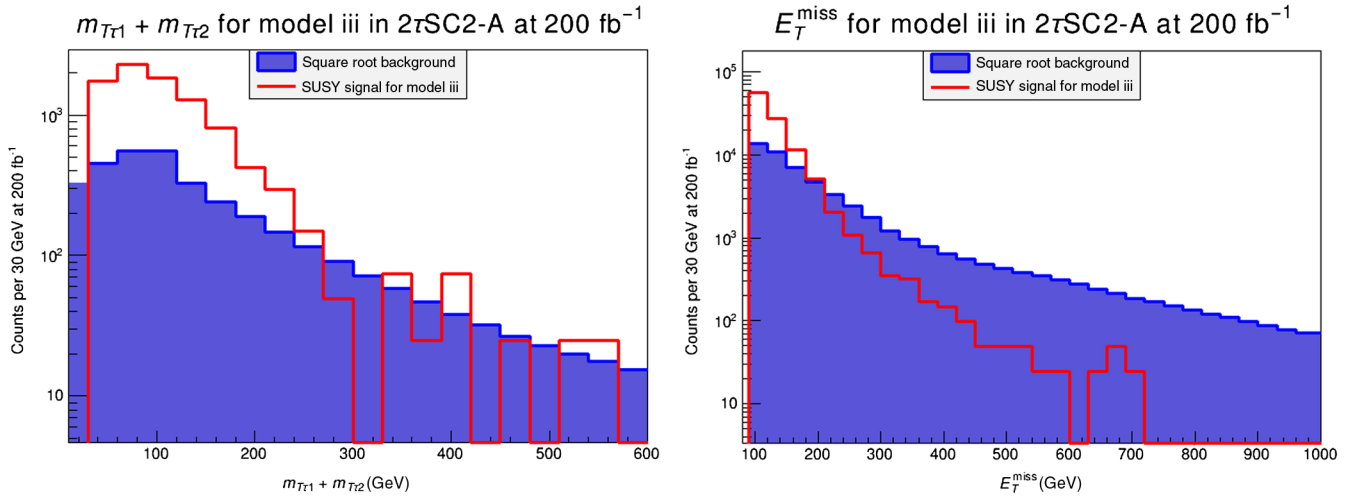

FIG. 9. (Left panel) Distribution in $m_{T\tau 1} + m_{T\tau 2}$ for the 2τSC2-A signal region for the multiparticle coannihilation model (iii) prior to any cuts. Plotted is the number of counts for the SUSY signal per 30 GeV and the square root of the total SM Snowmass backgrounds. The analysis is done at 200 fb^{-1} of integrated luminosity, which gives a 5σ discovery in this signal region. (Right panel) The same analysis as in the left panel but for E_T^{miss} with counts for the SUSY signal per 30 GeV.

are required to comprise a SFOS pair, with the third lepton allowed to have the same or a different flavor. For the case where all three leptons are the same flavor, the SFOS pair is chosen to be that whose invariant mass is closest to the Z mass. The three lepton case admits two signal regions, A and B, with B representing tighter cuts on relevant kinematic variables (see Table XIX). Here, in addition to a veto on b-tagged jets, cuts are applied to the missing transverse energy, the transverse momentum of the third lepton, the transverse mass as defined above, and the invariant mass of the SFOS pair.

With these signal regions, it is possible to assess the discovery potential of stau coannihilation region parameter points based on the signal from electroweak gaugino decays. Tables XX, XXI, and XXII below describe the results in terms of the integrated luminosity in fb^{-1} required for a 5σ discovery. Results for the three lepton signal regions described in Table XIX are not displayed because it was found that in all cases, the required luminosity for discovery was much larger than for the two lepton cases, indeed larger than the 3000 fb^{-1}. This is due to the fact that the decay events from these coannihilation regions almost never produce three final state leptons. We find that for the leptonic signal regions, as mentioned earlier it is only the two lepton signals that give promising results. Of these, the signal regions which require a SFOS pair perform much

TABLE XVIII. The selection criteria used for the signal regions related to the two lepton signature, based upon the two lepton signal regions from [42]. Here and in the tables following SF stands for same flavor, opposite sign lepton pair and DF stands for different flavor, opposite sign lepton pair. An empty cell denotes a cut which is not applicable to the given signal region.

	SF			DF		
Requirement	2l-SF-A	2l-SF-B	2l-SF-C‘	2l-DF-A	2l-DF-B	2l-DF-C
$E_T^{\text{miss}}(\text{GeV})>$	100	100	100	100	100	100
light jet $p_T(\text{GeV})<$	20	20	20	30	30	30
b-jet $p_T(\text{GeV})<$	20	20	20	20	20	20
forward jet $p_T(\text{GeV})<$	30	30	30	30	30	30
$\lvert m_{\ell\ell}-m_Z\rvert(\text{GeV})>$	10	10	10			
$m_{T2}(\text{GeV})>$	90	120	150	90	120	150

TABLE XIX. The selection criteria used for the signal regions related to the three lepton signature, based upon the two lepton signal regions from [42].

Requirement	Value	
	3l-A	3l-B
$E_T^{\text{miss}}(\text{GeV})>$	120	100
$p_T(\ell_3)(\text{GeV})>$	30	80
$m_T(\text{GeV})<$	110	110
$m_{\text{SFOS}}(\text{GeV})$	$\notin[21.2, 101.2]$	>101.2
$N(b\text{-jet})$	0	0

TABLE XX. Analysis of the discovery potential for supersymmetry for the parameter space of Table I, using the two lepton same flavor (SF) selection criteria of Table XVIII, where the minimum integrated luminosity needed for 5σ discovery is given in fb^{-1}. The different flavor (DF) signal regions are omitted due to poor performance (i.e., requiring over 3000 fb^{-1} of integrated luminosity for discovery).

	$\mathcal{L}$ for 5σ discovery in 2l-SF		
Model	2l-SF-A	2l-SF-B	2l-SF-C
(a)	187	266	266
(b)	362	420	441
(c)	165	188	169
(d)	781	953	884
(e)	1480	1630	1700
(f)	1110	1380	1250
(g)	1850	1850	1790
(h)	1860	2050	1660
(j)	2160	2250	1880
(k)	97	185	225

better than those requiring a DFOS pair. Thus, this specific signal region topology is found to be the best leptonic signal for the stau and multiparticle coannihilation regions. The remaining variation is upon kinematic cuts, in this case the cut on the variable m_{T2}. As expected for a kinematic cut, the softer cut of 2l-SF-A is optimal

TABLE XXI. Analysis of the discovery potential for supersymmetry for the parameter space of Table III, using the two lepton same flavor (SF) selection criteria of Table XVIII, where the minimum integrated luminosity needed for 5σ discovery is given in fb^{-1}. The different flavor (DF) signal regions are omitted due to poor performance (i.e., requiring over 3000 fb^{-1} of integrated luminosity for discovery). Model (x) is not listed because the minimum integrated luminosity needed for a 5σ discovery exceeded 3000 fb^{-1}.

	$\mathcal{L}$ for 5σ discovery in 2l-SF		
Model	2l-SF-A	2l-SF-B	2l-SF-C
(i)	545	623	696
(ii)	315	306	273
(iii)	181	271	238
(iv)	640	843	934
(v)	1410	1460	1690
(vi)	1090	1610	1500
(vii)	944	1450	1510
(viii)	732	1090	1190
(ix)	360	487	624
(xi)	224	450	547

TABLE XXII. Integrated luminosity for SUSY production in the leading and subleading leptonic (e and μ) signal regions of Tables XVIII and XIX for the benchmark points of Tables I and III.

Model	Leading SR	$\mathcal{L}$ (fb^{-1})	Model	Leading SR	$\mathcal{L}$ (fb^{-1})
(a)	2l-SF-A	187	(i)	2l-SF-A	454
(b)	2l-SF-A	362	(ii)	2l-SF-C	273
(c)	2l-SF-A	165	(iii)	2l-SF-A	181
(d)	2l-SF-A	781	(iv)	2l-SF-A	640
(e)	2l-SF-A	1480	(v)	2l-SF-A	1410
(f)	2l-SF-A	1110	(vi)	2l-SF-A	1090
(g)	2l-SF-C	1790	(vii)	2l-SF-A	944
(h)	2l-SF-C	1660	(viii)	2l-SF-A	732
(j)	2l-SF-C	1880	(ix)	2l-SF-A	360
(k)	2l-SF-A	97	(x)	2l-SF-C	⋯
			(xi)	2l-SF-A	224

for lower mass benchmark points, while the harder cut 2l-SF-C is optimal for higher mass points. The intermediate signal region 2l-SF-B was not optimal for any case studied. Figures 10 and 11 display the m_{T2} and E_T^{miss} kinematic variables for signal and combined background after cuts. Figure 10 gives counts in m_{T2} after the 2l-SF-A signal region cuts for models (k) and (c), models for which that signal region is optimal, displayed at the integrated luminosity calculated as necessary for discovery. Figure 11 gives counts in the same signal region and for the same models, but this time in the E_T^{miss} kinematic variable.

C. Combined signal region results

As an overall view of the signal regions considered and their success in discriminating between signal and background, we list in Tables XXIII and XXIV the leading and subleading signal regions and the corresponding model points for the stau and multiparticle coannihilation regions, respectively. Model points are listed in an ascending order of luminosity. The analysis of Tables XXIII and XXIV shows that probing the supersymmetric signals originating from the stau coannihilation and multiparticle coannihilation regions would be challenging. By the end of this year the CMS experiment is expected to collect about

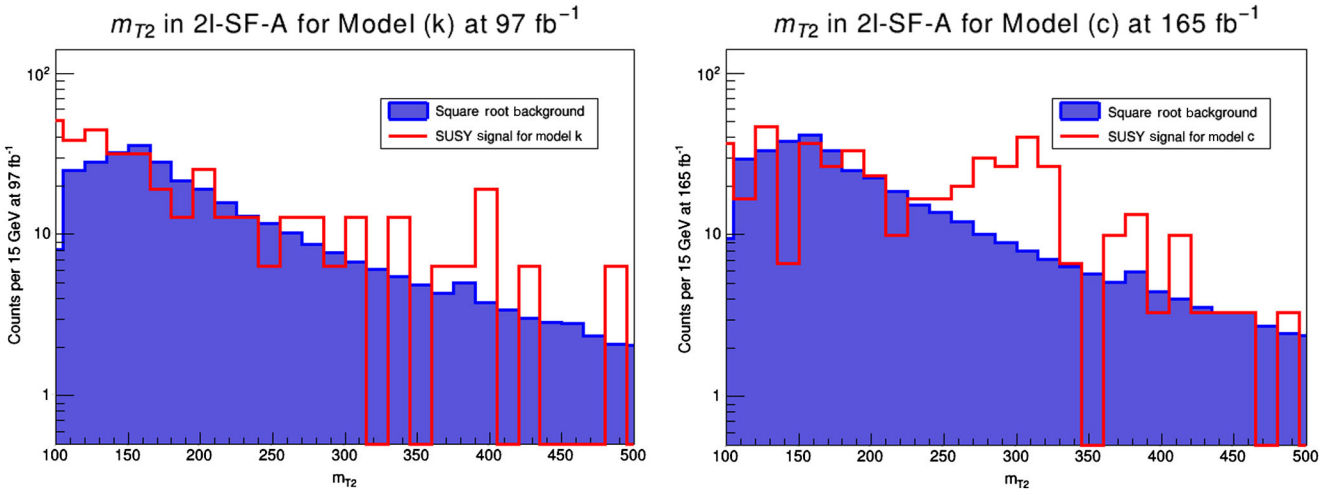

FIG. 10. (Left panel) Distribution in m_{T2} for the 2l-SF-A signal region defined in Table XVIII for stau coannihilation model (k) after cuts in that region. Plotted is the number of counts for the SUSY signal per 15 GeV and the square root of the total standard model Snowmass background. The analysis is done at 97 fb^{-1} of integrated luminosity, which gives a 5σ discovery in this signal region. (Right panel) The same analysis as in the left panel but for model (c) at 165 fb^{-1}.

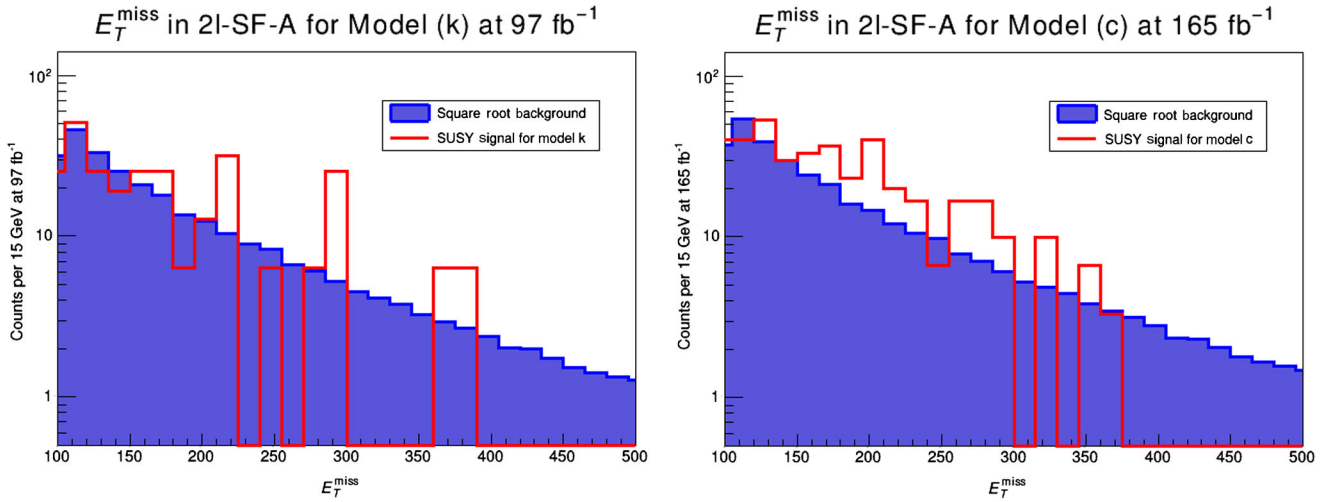

FIG. 11. (Left panel) Distribution in E_T^{miss} for the 2l-SF-A signal region defined in Table XVIII for stau coannihilation model (k) after cuts in that region. Plotted is the number of counts for the SUSY signal per 15 GeV and the square root of the total standard model Snowmass background. The analysis is done at 97 fb^{-1} of integrated luminosity, which gives a 5σ discovery in this signal region. (Right panel) The same analysis as in the left panel but for model (c) at 165 fb^{-1}.

TABLE XXIII. The overall minimum integrated luminosities needed for a 5σ discovery using the leading and subleading signal regions for stau coannihilation models of Table I, including the τ-based signal regions discussed in Sec. IV A as well as the e- and μ-based signal regions discussed in Sec. IV B.

Model	Leading SR	$\mathcal{L}$ (fb^{-1})	Subleading SR	$\mathcal{L}$ (fb^{-1})
(k)	2l-SF-A	97	2l-SF-B	185
(c)	2l-SF-A	165	2l-SF-C	169
(a)	2l-SF-A	187	2l-SF-B	266
(b)	2l-SF-A	362	1τ-SC2-C	416
(d)	2l-SF-A	781	2l-SF-C	884
(f)	2l-SF-A	1110	2l-SF-C	1250
(e)	2l-SF-A	1480	2l-SF-B	1630
(g)	2l-SF-C	1790	2l-SF-A	1850
(h)	2l-SF-C	1660	2l-SF-A	1860
(j)	2l-SF-C	1880	2l-SF-A	2160

45–50 fb^{-1} of data [58] and one expects similar amount of data from the ATLAS experiment [59]. One expects that by the time the LHC Run II is over one may have a large enough data set to probe part of the stau and multiparticle coannihilation regions—specifically model (k) of Table XXIII, which can be probed with 97 fb^{-1} of integrated luminosity, and model (xi) of Table XXIV, which can be probed with 73 fb^{-1} of integrated luminosity. Of course after the high luminosity LHC upgrade, HL-LHC is expected to collect up to 3 ab^{-1} of data at a center-of-mass energy of 14 TeV. Thus with this data the full set of models listed in Tables XXIII and XXIV can be tested. We note here that the dark matter constraints would become even more severe if the neutralino contributed only a fraction of the dark matter density in the Universe as is the case in multicomponent dark matter models (see e.g., [60]). One recent entry is the ultralight boson [61–63] needed to explain cosmology at small scales, which could contribute part of the relic density of dark matter. In this case the mass gaps between the neutralino and the stau would have to be even narrower to reduce the dark matter relic density to a fraction of the observed one. One item not addressed in this analysis and which needs further study is the effect of pileup (for a review of these effects see [64]). Such an analysis is outside the scope of the current work but could be a topic of further study.

TABLE XXIV. The overall minimum integrated luminosities needed for a 5σ discovery using the leading and subleading signal regions for the multiparticle coannihilation models of Table III, including the τ-based signal regions discussed in Sec. IV A as well as the e- and μ-based signal regions discussed in Sec. IV B.

Model	Leading SR	$\mathcal{L}$ (fb^{-1})	Subleading SR	$\mathcal{L}$ (fb^{-1})	Subleading leptonic SR	$\mathcal{L}$ (fb^{-1})
(xi)	2τ-SC2-A	73	2τ-SC2-B	89	2l-SF-A	224
(iii)	2l-SF-A	181	2τ-SC2-A	200	2l-SF-C	238
(ii)	2l-SF-C	273	2l-SF-B	306	2l-SF-B	306
(ix)	2l-SF-A	360	2l-SF-B	487	2l-SF-B	487
(v)	1τ-SC1-C	411	1τ-SC2-B	475	2l-SF-A	1410
(i)	2τ-SC2-A	477	2l-SF-A	545	2l-SF-A	454
(vii)	1τ-SC1-C	508	1τ-SC1-B	605	2l-SF-A	944
(iv)	1τ-SC1-C	532	1τ-SC1-B	575	2l-SF-A	640
(vi)	1τ-SC1-C	650	1τ-SC2-C	693	2l-SF-A	1090
(viii)	1τ-SC1-C	660	2l-SF-A	732	2l-SF-A	732
(x)	1τ-SC1-C	1090	1τ-SC1-B	1230	…	…

Next we compare our analysis with that of the recent analysis of the ATLAS Collaboration [42]. To begin with we note that the analysis of [42] is based on simplified models, and the details of these models in terms of the relative ratios of the sleptons and the electroweak gauginos are very different from the ones that arise in our analysis, which is based on a high scale model. This also applies to the branching ratios of the decays of the electroweak gauginos used by [42], which are again very different from our case. Thus some of the regions excluded in the analysis of [42] are not excluded for the high-scale models we consider.

In a further comparison of our analysis with that of [42], we note that throughout our analysis we use the full SUSY production cross sections. Thus the total sfermion production cross section includes the electroweak gaugino, stau, and slepton ($\tilde{e}$, $\tilde{\mu}$) production cross sections. We first compare our results of Table II based on the parameter set of Table I with the exclusion plots of Fig. 7 of [42]. The analysis of Fig. 7 of Ref. [42] uses a common first two generation slepton mass of $(m_{\tilde{\chi}_1^0} + m_{\chi_1^+})/2$. Further, they assume a 100% branching ratio of the decay of the chargino into sleptons. Neither of these assumptions are valid for the parameter points of Table I and the spectrum it generates as given by Table III. In any case the chargino and the neutralino mass spectrum of Table II lies outside the blue area adjoining the y axis in Fig. 7(a) and is thus not excluded. Further, there are no significant three lepton signals for the cases we consider and thus the analysis of Fig. 7(b) of Ref. [42] does not apply. So in this case the analysis of [42] and our analysis are in agreement regarding the parameter points of Table I and the spectrum of Table III, which are not excluded by the current data.

Next we consider the parameter set of Table III and the corresponding sparticle spectrum given by Table IV. Essentially all the observations made in the context of Tables I and II are also valid in this case. Specifically we can see from Table IV that the masses of $\tilde{e}_L$, $\tilde{e}_R$, $\tilde{\mu}_L$, $\tilde{\mu}_R$ are significantly higher than the chargino mass and thus the chargino can only decay into the light stau; it has no branching ratio into sleptons. In contrast the analysis of [42] assumes 100% branching ratio into $\tilde{e}$, $\tilde{\mu}$ sleptons and therefore its exclusion plots do not apply to our analysis. Specifically most of the parameter points of Tables III and IV lie inside the blue excluded region of Fig. 7(a) of [42], pointing to the danger of using simplified models which are

based on *ad hoc* assumptions and do not arise from any underlying theory to exclude valid regions of the parameter space of supergravity models.

We made further checks on our analysis. Most of the multiparticle coannihilation points (Table III) have a suppressed production cross section for sleptons. For example, for point (i) the total SUSY production cross section is 3.99 pb, which as we mentioned is dominated by the production of $\tilde{\chi}^{\pm}$ and $\tilde{\chi}^0_2$. Of the 3.99 pb, the sfermion production cross section is 0.161 pb, of which the production of staus comprises 0.1 pb and the production of sleptons comprises 0.061 pb. There are some exceptions: for example for point (iii) of Table IV, the total cross section is 6.17 pb, with the sfermion production cross section making around 0.14 pb of the total production cross section. Of the 0.14 pb, 0.073 pb goes for the production of staus and 0.067 for the sleptons. Here the production of sleptons is comparable to the staus, explaining the strong lepton signal in the final state for this point. The sixth column of Table XXIV shows the subleading leptonic signal region which, for some points, gives integrated luminosities comparable to that of the leading and subleading hadronic signal regions. Note that the production cross section of sleptons is less that staus since they are heavier.

As a further check on why the analysis of [42] is invalid in our case, we consider point (xi), which has the lightest LSP with a mass of 89.9 GeV and a chargino of mass 131.5 GeV. Following [42] we take the slepton masses to be as assumed by ATLAS. To get the relic density we require the mass gap between the chargino and neutralino to be around 20 GeV and their average to be the slepton mass (246 GeV in this case). Then a simple calculation leads to chargino and neutralino masses of ∼256 and ∼236 GeV. Referring to Fig. 7 of [42] we see that this parameter point is not excluded. A similar analysis can be carried out for the parameter set of Table I and the corresponding sparticle spectrum of Table II. Taking the lightest point of the spectrum, namely, point (k) and following the assumption of [42] regarding the slepton, chargino, and neutralino mass and requiring a mass gap of around 20 GeV, we find chargino and neutralino masses of ∼254 and 234 GeV, respectively, which according to Fig. 7 of [42] are not excluded. For this set of stau coannihilation points, as discussed above, the full SUSY cross section has been calculated and used in our analysis. Also for point (k), we found that the production cross section of electroweak gauginos is the dominant process making up 2.4 pb of the total cross section 2.65 pb. The direct stau production cross section amounts to 0.144 pb, while that of the slepton is 0.105 pb. It is clear that the slepton cross section is less than that of the stau but nonetheless not insignificant. An example of a slepton production cross section which is comparable to that of the stau can be seen for point (j). For this point, the production cross section of staus is 0.01 pb, while that of sleptons is 0.011 pb, which clearly shows that a signal of leptons in the final state would compete with that of the tau.

We note that the simulation of the SUSY signals was performed at 14 TeV to match the Snowmass SM backgrounds. If one considers 13 TeV, then, as an example, for point (x) of Table III one gets a production cross section of 1.44 instead of 1.63 pb. As for point (xi), one gets 9.19 pb instead of 10.19 pb. Thus there is around a 10% difference, which one supposes would not have a major impact on the 5σ discovery limit on integrated luminosity. It is not possible, however, to predict the exact integrated luminosity for a 5σ discovery at 13 TeV since the Snowmass SM backgrounds are not available at 13 TeV.

Next we give a comparison of our work with that of a previous analysis [43] which carried out simulations of the $\tilde{g}$SUGRA model. A direct comparison of our results with that of [43] is difficult because of the following reasons: (i) The analysis of [43] gives only scatter plots in the space of sparticle masses and of the input parameters, whereas we work with a list of benchmarks. (ii) The analysis of [43] is done at 300 fb^{-1} in Fig. 9 of that work at 14 TeV, while our analysis at 14 TeV looks for minimum integrated luminosity for a 5σ discovery limit. (iii) We have carried out an optimization of the signal regions for a SUSY discovery focused on the model points considered but it is not clear what has been done in this regard in the analysis of [43]. However, with these caveats a comparison of this work with that of [43], where possible, shows consistency between the two analyses.

D. Stau coannihilation and direct detection of dark matter

The analysis presented in Tables XXIII and XXIV give us a set of models which are consistent with the Higgs boson mass constraint and the constraints on the relic density consistent with the WMAP [65] and the Planck experiment [66] and arise from the stau or stau–chargino–second neutralino coannihilation regions. It is of interest to investigate if these models are discoverable in a direct detection experiment. For these models the neutralino is mostly a bino. Thus the neutralino is a linear combination of four states $\tilde{\chi}^0 = \alpha\lambda^0 + \beta\lambda^3 + \gamma\tilde{H}_1 + \delta\tilde{H}_2$, where λ^0, λ^3 are the bino, wino and $\tilde{H}_1$, $\tilde{H}_2$ are the Higgsinos. For the models of Table I, $|\beta| \leq 0.003$, $|\gamma| \leq 0.015$, $|\delta| \leq 0.002$, while for the models of Table III, $|\beta| \leq 0.039$, $|\gamma| \leq 0.014$, $|\delta| \leq 0.002$. One finds that the wino and the Higgsino content of the models of Tables I and III are small, and the neutralino is essentially a bino. This makes the neutralino-proton cross sections relatively small. In Table XXV we present the spin-independent and spin-dependent neutralino-proton cross sections for these models. The analysis of Table XXV shows that the spin-independent neutralino-proton cross section though small and $O(10^{48}\ \text{cm}^{-2})$ still lies significantly above the neutrino floor [67], which is the

TABLE XXV. (Three upper columns) Proton-neutralino spin-independent ($\sigma^{SI}_{p\tilde{\chi}^0_1}$) and spin-dependent ($\sigma^{SD}_{p\tilde{\chi}^0_1}$) cross sections in units of cm^{-2} for the ten benchmark points of Table I. (Three lower columns) Proton-neutralino spin-independent ($\sigma^{SI}_{p\tilde{\chi}^0_1}$) and spin-dependent ($\sigma^{SD}_{p\tilde{\chi}^0_1}$) cross sections in units of cm^{-2} for the 11 benchmark points of Table III.

Model	$\sigma^{SI}_{p\tilde{\chi}^0_1} \times 10^{48}$	$\sigma^{SD}_{p\tilde{\chi}^0_1} \times 10^{46}$
(a)	0.92	4.77
(b)	0.80	3.67
(c)	1.08	5.60
(d)	0.80	6.35
(e)	0.58	4.43
(f)	0.64	4.82
(g)	0.40	2.39
(h)	0.27	1.03
(j)	0.53	3.52
(k)	1.22	0.25

Model	$\sigma^{SI}_{p\tilde{\chi}^0_1} \times 10^{48}$	$\sigma^{SD}_{p\tilde{\chi}^0_1} \times 10^{45}$
(i)	1.33	3.02
(ii)	1.97	3.54
(iii)	0.94	1.03
(iv)	1.94	2.87
(v)	1.74	2.45
(vi)	2.90	5.66
(vii)	1.46	1.93
(viii)	2.02	3.28
(ix)	0.96	1.88
(x)	3.01	4.77
(xi)	1.11	1.53

minimum threshold for detectability (see Fig. 12). Some of the models also lie close to the lower bounds that the future dark matter experiments LUX-ZEPLIN [68,69] could be able to reach.

V. CONCLUSIONS

Supersymmetry is desirable for a number of theoretical as well as phenomenological reasons. Supergravity unification provides a framework for high-scale models with a small number of parameters in terms of which the properties of low energy effective theory can be computed. The observation of the Higgs boson mass at ∼125 GeV implies that the loop correction to the tree level Higgs boson mass is large which in turn implies that the scale of weak scale supersymmetry lies in the TeV region. This makes the search for supersymmetry more challenging than initially thought. For high-scale models, there is another aspect which makes the observation of supersymmetry challenging. This concerns dark matter. For high-scale models one finds that often the parameter space that gives the desired Higgs boson mass gives a neutralino which is mostly a bino. For a bino-type neutralino, one needs coannihilation to achieve the appropriate relic density consistent with the WMAP and the Planck experiment. This means that there must be one or more sparticles close by to coannihilate with the neutralino. The relatively small mass gap between the neutralino and the coannihilating particles implies that the final states in the decay of the coannihilating particles must be soft and thus hard to detect. In this work we have addressed this question in the context of stau coannihilation. We have analyzed two types of models: one type which involves only a two particle coannihilation between the neutralino and the stau, and the second type where the neutralino coannihilates with a stau, a chargino, and a second neutralino. We have carried out an extensive signature analysis including a variety of signatures including one tau and two tau final states as well as e and μ final states. Our analysis shows that a variety of signatures exist where the neutralino-stau coannihilation

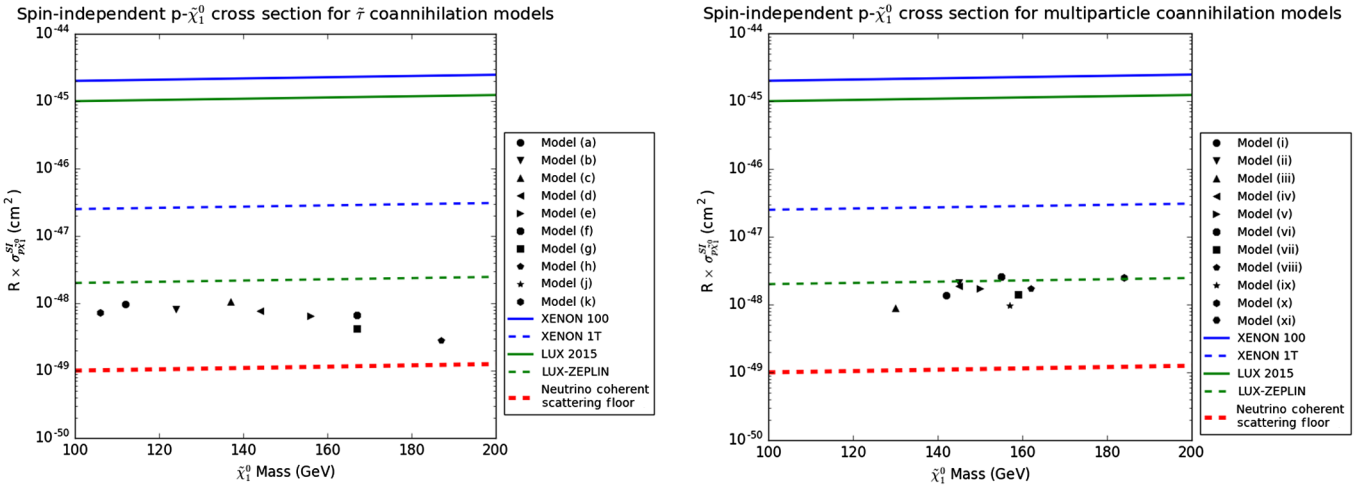

FIG. 12. $R \times \sigma^{SI}_{p\tilde{\chi}^0_1} (R = \rho_{\tilde{\chi}^0_1}/\rho_c)$ for models of Tables I (left panel) and III (right panel) as a function of LSP mass displayed alongside the current and projected range of the XENON and LUX experiments and the neutrino floor.

and the neutralino–stau–chargino–second neutralino coannihilation can be discovered with the total integrated luminosity expected at the LHC in the future. We have also analyzed the spin-independent neutralino-proton cross section. It is found that the cross section lies significantly above the neutrino floor and some parts of the parameter space may be accessible in future dark matter experiments such as LUX and ZEPLIN and XENON1T.

ACKNOWLEDGMENTS

Computational time allocation at the high-performance Cluster353 at the Advanced Scientific Computing Initiative (ASCI) and the Discovery Cluster at Northeastern University is acknowledged. Also acknowledged are conversations with Bhaskar Dutta, Toyoko Orimoto, and Baris Altunkaynak. This research was supported in part by NSF Grants No. PHY-1314774 and No. PHY-1620575.

[1] F. Englert and R. Brout, Broken Symmetry and the Mass of Gauge Vector Mesons, Phys. Rev. Lett. **13**, 321 (1964).
[2] P. W. Higgs, Broken Symmetries and the Masses of Gauge Bosons, Phys. Rev. Lett. **13**, 508 (1964).
[3] G. S. Guralnik, C. R. Hagen, and T. W. B. Kibble, Global Conservation Laws and Massless Particles, Phys. Rev. Lett. **13**, 585 (1964).
[4] S. Chatrchyan *et al.* (CMS Collaboration), Observation of a new boson at a mass of 125 GeV with the CMS experiment at the LHC, Phys. Lett. B **716**, 30 (2012).
[5] G. Aad *et al.* (ATLAS Collaboration), Observation of a new particle in the search for the standard model Higgs boson with the ATLAS detector at the LHC, Phys. Lett. B **716**, 1 (2012).
[6] P. Nath, Supersymmetry after the Higgs, Ann. Phys. (Amsterdam) **528**, 167 (2016).
[7] A. H. Chamseddine, R. Arnowitt, and P. Nath, Locally Supersymmetric Grand Unification, Phys. Rev. Lett. **49**, 970 (1982); P. Nath, R. L. Arnowitt, and A. H. Chamseddine, Gauge hierarchy in supergravity GUTs, Nucl. Phys. **B227**, 121 (1983); L. J. Hall, J. D. Lykken, and S. Weinberg, Supergravity as the messenger of supersymmetry breaking, Phys. Rev. D **27**, 2359 (1983).
[8] P. Nath, *Supersymmetry, Supergravity, and Unification* (Cambridge University Press, Cambridge, England, 2016).
[9] S. Akula, B. Altunkaynak, D. Feldman, P. Nath, and G. Peim, Higgs boson mass predictions in SUGRA unification, recent LHC-7 results, and dark matter, Phys. Rev. D **85**, 075001 (2012).
[10] A. Arbey, M. Battaglia, A. Djouadi, and F. Mahmoudi, The Higgs sector of the phenomenological MSSM in the light of the Higgs boson discovery, J. High Energy Phys. 09 (2012) 107.
[11] H. Baer, V. Barger, and A. Mustafayev, Implications of a 125 GeV Higgs scalar for LHC SUSY and neutralino dark matter searches, Phys. Rev. D **85**, 075010 (2012); A. Arbey, M. Battaglia, A. Djouadi, F. Mahmoudi, and J. Quevillon, Implications of a 125 GeV Higgs for supersymmetric models, Phys. Lett. B **708**, 162 (2012); P. Draper, P. Meade, M. Reece, and D. Shih, Implications of a 125 GeV Higgs for the MSSM and low-scale SUSY breaking, Phys. Rev. D **85**, 095007 (2012); M. Carena, S. Gori, N. R. Shah, and C. E. M. Wagner, A 125 GeV SM-like Higgs in the MSSM and the $\gamma\gamma$ rate, J. High Energy Phys. 03 (2012) 014; O. Buchmueller *et al.*, Higgs and supersymmetry, Eur. Phys. J. C **72**, 2020 (2012); S. Akula, P. Nath, and G. Peim, Implications of the Higgs boson discovery for mSUGRA, Phys. Lett. B **717**, 188 (2012); C. Strege, G. Bertone, F. Feroz, M. Fornasa, R. Ruiz de Austri, and R. Trotta, Global Fits of the cMSSM and NUHM including the LHC Higgs discovery and new XENON100 constraints, J. Cosmol. Astropart. Phys. 04 (2013) 013.
[12] H. Baer, V. Barger, and M. Savoy, Supergravity gauge theories strike back: There is no crisis for SUSY but a new collider may be required for discovery, Phys. Scr. **90**, 068003 (2015).
[13] R. L. Arnowitt and P. Nath, SUSY Mass Spectrum in SU(5) Supergravity Grand Unification, Phys. Rev. Lett. **69**, 725 (1992).
[14] K. Griest and D. Seckel, Three exceptions in the calculation of relic abundances, Phys. Rev. D **43**, 3191 (1991).
[15] D. Feldman, Z. Liu, and P. Nath, Landscape of Supersymmetric Particle Mass Hierarchies and Their Signature Space at the Large Hadron Collider, Phys. Rev. Lett. **99**, 251802 (2007); Errattum, Phys. Rev. Lett. **100**, 069902(E) (2008); Light Higgses at the Tevatron and at the LHC and observable dark matter in SUGRA and *D* branes, Phys. Lett. B **662**, 190 (2008); Sparticles at the LHC, J. High Energy Phys. 04 (2008) 054; N. Chen, D. Feldman, Z. Liu, P. Nath, and G. Peim, Low mass gluino within the sparticle landscape, implications for dark matter, and early discovery prospects at LHC-7, Phys. Rev. D **83**, 035005 (2011); D. Francescone, S. Akula, B. Altunkaynak, and P. Nath, Sparticle mass hierarchies, simplified models from SUGRA unification, and benchmarks for LHC Run-II SUSY searches, J. High Energy Phys. 01 (2015) 158.
[16] J. R. Ellis, K. Enqvist, D. V. Nanopoulos, and K. Tamvakis, Gaugino masses and grand unification, Phys. Lett. **155B**, 381 (1985).
[17] A. Corsetti and P. Nath, Gaugino mass nonuniversality and dark matter in SUGRA, strings and *D* brane models, Phys. Rev. D **64**, 125010 (2001); U. Chattopadhyay and P. Nath, $b-\tau$ unification, $g_\mu-2$, the $bs+\gamma$ constraint and nonuniversalities, Phys. Rev. D **65**, 075009 (2002); A. Birkedal-Hansen and B. D. Nelson, Relic neutralino densities and detection rates with nonuniversal gaugino masses, Phys. Rev. D **67**, 095006 (2003); U. Chattopadhyay and D. P. Roy, Higgsino dark matter in a SUGRA model with nonuniversal

gaugino masses, Phys. Rev. D **68**, 033010 (2003); D. G. Cerdeno and C. Munoz, Neutralino dark matter in supergravity theories with non-universal scalar and gaugino masses, J. High Energy Phys. 10 (2004) 015; G. Belanger, F. Boudjema, A. Cottrant, A. Pukhov, and A. Semenov, WMAP constraints on SUGRA models with non-universal gaugino masses and prospects for direct detection, Nucl. Phys. **B706**, 411 (2005); H. Baer, A. Mustafayev, E. K. Park, S. Profumo, and X. Tata, Mixed Higgsino dark matter from a reduced SU(3) gaugino mass: Consequences for dark matter and collider searches, J. High Energy Phys. 04 (2006) 041; K. Choi and H. P. Nilles, The gaugino code, J. High Energy Phys. 04 (2007) 006; I. Gogoladze, R. Khalid, N. Okada, and Q. Shafi, Soft probes of SU(5) unification, Phys. Rev. D **79**, 095022 (2009); S. Bhattacharya, A. Datta, and B. Mukhopadhyaya, Non-universal gaugino and scalar masses, hadronically quiet trileptons and the Large Hadron Collider, Phys. Rev. D **78**, 115018 (2008); M. E. Gomez, S. Lola, P. Naranjo, and J. Rodriguez-Quintero, WMAP dark matter constraints on Yukawa unification with massive neutrinos, J. High Energy Phys. 04 (2009) 043; B. Altunkaynak, P. Grajek, M. Holmes, G. Kane, and B. D. Nelson, Studying gaugino mass unification at the LHC, J. High Energy Phys. 04 (2009) 114; U. Chattopadhyay, D. Das, and D. P. Roy, Mixed neutralino dark matter in nonuniversal gaugino mass models, Phys. Rev. D **79**, 095013 (2009); S. Bhattacharya and J. Chakrabortty, Gaugino mass non-universality in an SO(10) supersymmetric grand unified theory: Low-energy spectra and collider signals, Phys. Rev. D **81**, 015007 (2010); S. P. Martin, Nonuniversal gaugino masses from nonsinglet F-terms in nonminimal unified models, Phys. Rev. D **79**, 095019 (2009).

[18] D. Matalliotakis and H. P. Nilles, Implications of non-universality of soft terms in supersyrnmetric grand unified theories, Nucl. Phys. **B435**, 115 (1995); M. Olechowski and S. Pokorski, Electroweak symmetry breaking with non-universal scalar soft terms and large tanβ solutions, Phys. Lett. B **344**, 201 (1995); N. Polonski and A. Pomerol, Nonuniversal GUT corrections to the soft terms and their implications in supergravity models, Phys. Rev. D **51**, 6532 (1995); P. Nath and R. Arnowitt, Nonuniversal soft SUSY breaking and dark matter, Phys. Rev. D **56**, 2820 (1997); E. Accomando, R. L. Arnowitt, B. Dutta, and Y. Santoso, Neutralino proton cross-sections in supergravity models, Nucl. Phys. **B585**, 124 (2000); J. R. Ellis, K. A. Olive, and Y. Santoso, The MSSM parameter space with non-universal Higgs masses, Phys. Lett. B **539**, 107 (2002); H. Baer, A. Mustafayev, S. Profumo, A. Belyaev, and X. Tata, Direct, indirect and collider detection of neutralino dark matter in SUSY models with non-universal Higgs masses, J. High Energy Phys. 07 (2005) 065; U. Chattopadhyay and D. Das, Higgs funnel region of SUSY dark matter for small tan β and renormalization group effects on pseudoscalar Higgs boson with scalar mass nonuniversality, Phys. Rev. D **79**, 035007 (2009).

[19] K. L. Chan, U. Chattopadhyay, and P. Nath, Naturalness, weak scale supersymmetry and the prospect for the observation of supersymmetry at the Tevatron and at the CERN LHC, Phys. Rev. D **58**, 096004 (1998).

[20] J. L. Feng, K. T. Matchev, and T. Moroi, Multi-TeV Scalars are Natural in Minimal Supergravity, Phys. Rev. Lett. **84**, 2322 (2000).

[21] U. Chattopadhyay, A. Corsetti, and P. Nath, WMAP constraints, supersymmetric dark matter, and implications for the direct detection of supersymmetry, Phys. Rev. D **68**, 035005 (2003).

[22] H. Baer, C. Balazs, A. Belyaev, T. Krupovnickas, and X. Tata, Updated reach of the CERN LHC and constraints from relic density, $b \to s\gamma$ and a(μ) in the mSUGRA model, J. High Energy Phys. 06 (2003) 054.

[23] D. Feldman, G. Kane, E. Kuflik, and R. Lu, A new (string motivated) approach to the little hierarchy problem, Phys. Lett. B **704**, 56 (2011).

[24] S. Akula, M. Liu, P. Nath, and G. Peim, Naturalness, supersymmetry and implications for LHC and dark matter, Phys. Lett. B **709**, 192 (2012).

[25] G. G. Ross, K. Schmidt-Hoberg, and F. Staub, Revisiting fine-tuning in the MSSM, J. High Energy Phys. 03 (2017) 021.

[26] P. Nath and P. Fileviez Perez, Proton stability in grand unified theories, in strings and in branes, Phys. Rep. **441**, 191 (2007).

[27] M. Liu and P. Nath, Higgs boson mass, proton decay, naturalness, and constraints of the LHC and Planck data, Phys. Rev. D **87**, 095012 (2013).

[28] B. Kaufman, P. Nath, B. D. Nelson, and A. B. Spisak, Light stops and observation of supersymmetry at LHC run II, Phys. Rev. D **92**, 095021 (2015).

[29] P. Nath and A. B. Spisak, Gluino coannihilation and observability of gluinos at LHC run II, Phys. Rev. D **93**, 095023 (2016).

[30] J. Dutta, P. Konar, S. Mondal, B. Mukhopadhyaya, and S. K. Rai, A revisit to a compressed supersymmetric spectrum with 125 GeV Higgs, J. High Energy Phys. 01 (2016) 051.

[31] M. Berggren, A. Cakir, D. Krcker, J. List, I. A. Melzer-Pellmann, B. Safarzadeh Samani, C. Seitz, and S. Wayand, Non-simplified SUSY: $\tilde{\tau}$-coannihilation at LHC and ILC, Eur. Phys. J. C **76**, 183 (2016).

[32] M. Berggren, SUSY model and dark matter determination in the compressed-spectrum region at the ILC, *Proc. Sci.*, ICHEP2016 (2016) 154 [arXiv:1611.04450].

[33] T. J. LeCompte and S. P. Martin, Compressed supersymmetry after 1/fb at the Large Hadron Collider, Phys. Rev. D **85**, 035023 (2012); Large Hadron Collider reach for supersymmetric models with compressed mass spectra, Phys. Rev. D **84**, 015004 (2011).

[34] V. Khachatryan *et al.* (CMS Collaboration), Search for Dark Matter and Supersymmetry with a Compressed Mass Spectrum in the Vector Boson Fusion Topology in Proton-Proton Collisions at $\sqrt{s} = 8$ TeV, Phys. Rev. Lett. **118**, 021802 (2017).

[35] V. Khachatryan *et al.* (CMS Collaboration), Search for top squark pair production in compressed-mass-spectrum scenarios in proton-proton collisions at $\sqrt{s} = 8$ TeV using the α_T variable, Phys. Lett. B **767**, 403 (2017).

[36] L. Morvaj (for the ATLAS Collaboration), Search for supersymmetry with a compressed mass spectrum in events involving soft leptons, jets and missing transverse momentum with an integrated luminosity of 20.1 pb^{-1} of $\sqrt{s} =$ 8 TeV ATLAS data, *Proc. Sci.*, EPS-HEP2013 (2013) 050.

[37] J. R. Ellis, T. Falk, and K. A. Olive, Neutralino-stau coannihilation and the cosmological upper limit on the mass of the lightest supersymmetric particle, Phys. Lett. B **444**, 367 (1998); J. R. Ellis, T. Falk, K. A. Olive, and M. Srednicki, Calculations of neutralino-stau coannihilation channels and the cosmologically relevant region of MSSM parameter space, Astropart. Phys. **13**, 181 (2000); Erratum, Astropart. Phys. **15**, 413(E) (2001).

[38] R. L. Arnowitt, B. Dutta, A. Gurrola, T. Kamon, A. Krislock, and D. Toback, Determining the Dark Matter Relic Density in the Minimal Supergravity Stau-Neutralino Coannihilation Region at the Large Hadron Collider, Phys. Rev. Lett. **100**, 231802 (2008); R. L. Arnowitt, A. Aurisano, B. Dutta, T. Kamon, N. Kolev, P. Simeon, D. A. Toback, and P. Wagner, Indirect measurements of the stau-neutralino 1 (0) mass difference and mSUGRA in the co-annihilation region of mSUGRA models at the LHC, Phys. Lett. B **649**, 73 (2007).

[39] J. E. Camargo-Molina, B. O'Leary, W. Porod, and F. Staub, Stability of the CMSSM against sfermion VEVs, J. High Energy Phys. 12 (2013) 103; J. E. Camargo-Molina, B. Garbrecht, B. O'Leary, W. Porod, and F. Staub, Constraining the natural MSSM through tunneling to color-breaking vacua at zero and non-zero temperature, Phys. Lett. B **737**, 156 (2014).

[40] A. Flórez, L. Bravo, A. Gurrola, C. Ávila, M. Segura, P. Sheldon, and W. Johns, Probing the stau-neutralino coannihilation region at the LHC with a soft tau lepton and a jet from initial state radiation, Phys. Rev. D **94**, 073007 (2016).

[41] S. Akula and P. Nath, Gluino-driven radiative breaking, Higgs boson mass, muon $g-2$, and the Higgs diphoton decay in supergravity unification, Phys. Rev. D **87**, 115022 (2013).

[42] ATLAS Collaboration, Report No. ATLAS-CONF-2016-096, 2016.

[43] K. Kowalska, L. Roszkowski, E. M. Sessolo, and A. J. Williams, GUT-inspired SUSY and the muon $g-2$ anomaly: Prospects for LHC 14 TeV, J. High Energy Phys. 06 (2015) 020.

[44] L. E. Ibanez and G. G. Ross, Supersymmetric Higgs and radiative electroweak breaking, C.R. Phys. **8**, 1013 (2007).

[45] B. C. Allanach, SOFTSUSY: A program for calculating supersymmetric spectra, Comput. Phys. Commun. **143**, 305 (2002).

[46] B. C. Allanach, S. P. Martin, D. G. Robertson, and R. Ruiz de Austri, The inclusion of two-loop SUSYQCD corrections to gluino and squark pole masses in the minimal and next-to-minimal supersymmetric standard model: SOFTSUSY3.7, arXiv:1601.06657.

[47] G. Blanger, F. Boudjema, A. Pukhov, and A. Semenov, MICROMEGAS4.1: two dark matter candidates, Comput. Phys. Commun. **192**, 322 (2015).

[48] A. Buckley, PYSLHA: A Pythonic interface to SUSY Les Houches Accord data, Eur. Phys. J. C **75**, 467 (2015).

[49] J. Alwall, R. Frederix, S. Frixione, V. Hirschi, F. Maltoni, O. Mattelaer, H.-S. Shao, T. Stelzer, P. Torrielli, and M. Zaro, The automated computation of tree-level and next-to-leading order differential cross sections, and their matching to parton shower simulations, J. High Energy Phys. 07 (2014) 079.

[50] A. Djouadi, M. M. Muhlleitner, and M. Spira, Decays of supersymmetric particles: The program SUSY-HIT (SUspect-SdecaY-Hdecay-InTerface), Acta Phys. Pol. B **38**, 635 (2007).

[51] T. Sjostrand, S. Mrenna, and P. Z. Skands, PYTHIA6.4 physics and manual, J. High Energy Phys. 05 (2006) 026.

[52] S. Ovyn, X. Rouby, and V. Lemaitre, DELPHES, a framework for fast simulation of a generic collider experiment, arXiv:0903.2225.

[53] R. Brun and F. Rademakers, ROOT: An object oriented data analysis framework, Nucl. Instrum. Methods Phys. Res., Sect. A **389**, 81 (1997).

[54] A. Avetisyan *et al.*, Methods and results for standard model event generation at $\sqrt{s} = 14$ TeV, 33 TeV and 100 TeV proton colliders (a Snowmass whitepaper), arXiv:1308.1636.

[55] C. G. Lester and D. J. Summers, Measuring masses of semiinvisibly decaying particles pair produced at hadron colliders, Phys. Lett. B **463**, 99 (1999).

[56] A. Barr, C. Lester, and P. Stephens, m_{T2}: The truth behind the glamour, J. Phys. G **29**, 2343 (2003).

[57] C. G. Lester and B. Nachman, Bisection-based asymmetric M_{T2} computation: A higher precision calculator than existing symmetric methods, J. High Energy Phys. 03 (2015) 100.

[58] See https://twiki.cern.ch/twiki/bin/view/CMSPublic/LumiPublicResults#2016_Proton_Proton_13_TeV_Collis and http://lpc.web.cern.ch/cgi-bin/plots.py.

[59] See https://twiki.cern.ch/twiki/bin/view/AtlasPublic/LuminosityPublicResultsRun2#Publications_and_Conference_Resu.

[60] D. Feldman, Z. Liu, P. Nath, and G. Peim, Multicomponent dark matter in supersymmetric hidden sector extensions, Phys. Rev. D **81**, 095017 (2010).

[61] L. Hui, J. P. Ostriker, S. Tremaine, and E. Witten, Ultralight scalars as cosmological dark matter, Phys. Rev. D **95**, 043541 (2017).

[62] D. J. E. Marsh, Axion cosmology, Phys. Rep. **643**, 1 (2016).

[63] J. Halverson, C. Long, and P. Nath, An ultralight axion in supersymmetry and strings and cosmology at small scales, arXiv:1703.07779.

[64] G. Aad *et al.* (ATLAS Collaboration), Performance of pile-up mitigation techniques for jets in pp collisions at $\sqrt{s} = 8$ TeV using the ATLAS detector, Eur. Phys. J. C **76**, 581 (2016).

[65] D. Larson *et al.*, Seven-year Wilkinson Microwave Anisotropy Probe (WMAP) observations: Power spectra and WMAP-derived parameters, Astrophys. J. Suppl. Ser. **192**, 16 (2011).

[66] P. A. R. Ade *et al.* (Planck Collaboration), Planck 2015 results. XIII. Cosmological parameters, Astron. Astrophys. **594**, A13 (2016).

[67] L. E. Strigari, Neutrino coherent scattering rates at direct dark matter detectors, New J. Phys. **11**, 105011 (2009).

[68] M. Schumann, Dark matter 2014, EPJ Web Conf. **96**, 01027 (2015).

[69] P. Cushman *et al.*, Snowmass CF1 summary: WIMP dark matter direct detection, arXiv:1310.8327.